Shock-wave structure according to a linear irreversible thermodynamic model

R. M. Velasco and F. J. Uribe*
Department of Physics, Universidad Autónoma Metropolitana–Iztapalapa, C.P. 09340, México D.F., México

(Received 17 December 2018; published 27 February 2019)

In this work we present a phenomenological model to look for a better understanding of the shock-wave structure in dilute monatomic gases. The model is based on the principles of linear irreversible thermodynamics, where we have been aware of the flow anisotropy caused by the shock-wave propagation. Then a new coupling appears between the stress tensor and the heat flux. The comparisons with the experimental data available for argon as well as the direct simulation Monte Carlo method calculations are done and shown to support our proposal.

DOI: 10.1103/PhysRevE.99.023114

I. INTRODUCTION

The description and understanding of the shock-wave profile has been a strong challenge for any set of continuum fluid mechanics equations. The main problem is the presence of a highly nonequilibrium flow where the usual variables have very deep changes in a short distance. Even though the flow is stationary, there are two dimensionless numbers which become essential in the characterization of the problem. The first one is the Mach number (M), which is the ratio between the wave speed and the sound speed in the fluid. The other one is the Knudsen number (Kn), defined as the quotient between the mean free path and the problem typical length; it measures the rarefaction of the system. The Mach number is greater than 1 and the Knudsen number value is in the so-called transition-continuum region, in such a way that the flow behavior is somewhat difficult to be treated with the usual tools in hydrodynamics. First, the Mach number value makes the flow a compressible one and, second, in the transition-continuum region the rarefaction in the system must be taken into account. In the understanding of the shock-wave structure, the comments we have made about the dimensionless numbers in this problem have given place to a numerous approaches. All of them drive to different schemes going from the kinetic to the phenomenological descriptions [1]. Most kinetic approaches begin with the Boltzmann equation and its methods of solution. A first example of the followed way is the Chapman-Enskog method, which corresponds to an expansion in powers of the Knudsen number. It gives us in the zeroth order, the Euler's equations giving a step solution when they are considered under the conditions for a shock wave. The first order in Knudsen number reproduces the Navier-Newton stress tensor and the Fourier law concerning the heat flux [2]. The second- and third-order solutions produce the Burnett [3,4] and super-Burnett [5]; all of them have been applied to study the shock-wave structure [6]. Also, Grad's method [7,8] with different numbers of momenta [9,10] and their modifications have been studied, for example, in Refs. [11,12]. The Mott-Smith formulation [13–15] is based on a bimodal distribution function where the subsonic properties are different from the supersonic ones. Also longitudinal and transversal temperatures have been taken in consideration according to a kinetic treatment [16–19]. All of them offered an alternative to understand some peculiarities in the problem; however, the predicted results do not agree completely with direct simulation Monte Carlo (DSMC) calculations [15] or some of the experimental data available [20–22].

On the other hand, the phenomenological approaches start with the steady fluxes of mass, momentum, and energy equations along the shock wave. They contain the equations of state and caloric and constitutive equations, where all of them must be given according to the fluid properties. Such constitutive equations can be the usual Navier-Newton and Fourier laws [21,23,24], the Cattaneo [25–27], and the Burnett [28,29]. Some modifications of them come from a different definition in the hydrodynamic velocity [30–33], the extended irreversible thermodynamics treatment [34–36], or generalized hydrodynamic studies [37–39]; even the moments methods allow the calculation of constitutive equations to obtain the closure needed to find the shock-wave profiles [9]. From the phenomenological point of view, the idea about longitudinal and transversal temperatures came to the fore through the Holian's conjecture [40]. In such a paper the molecular dynamics (MD) calculations indicated that for a strong shock, the Navier-Stokes-Fourier set of equations (NSF) give a better fit for density profiles obtained with MD calculations if the longitudinal temperature instead of the average one is taken to calculate the viscosity in the fluid. Then, a modification of NSF equations with the hard-sphere temperature dependence in the viscosity was considered taking Holian's conjecture [41]. A modification of the heat flux constitutive equation together with longitudinal temperature was assumed for strong shocks [42], obtaining some improvements. Some other papers have taken similar ideas with different constitutive constitutive equations, such as Cattaneo's relaxation and Burnett nonlinear contributions [25,43] among others.

*paco@xanum.uam.mx

In this paper we will be concerned deeply with the phenomenological approach for a dilute monatomic gas where the local equilibrium hypothesis is taken to write the pressure in terms of the density and temperature, and the energy is given by the local equipartition law consistently with ideal gas behavior. In contrast, the constitutive equations for the dissipative contributions such as the heat flux and the viscous tensor will be constructed following the lines of the principles of linear irreversible thermodynamics (LIT) and the flow anisotropy produced by shock-wave propagation. The motivation to undertake such a task comes from the enhancement in the viscosity coefficient observed in the NSF model which was complemented with a temperature dependence typical of the soft-sphere interaction between particles reported recently [1]. In such a paper we found that the NSF equations are capable of reproducing the normalized density profiles for several values of the Mach number by means of an index in the viscosity producing its enhancement. However, the performance of the results when compared with DSMC calculations and experimental data available was not so good for some other characteristics, like the orbit and the normalized temperature profile.

The main goal of this work will be the treatment of a set of equations obtained from the methods in LIT, with transport coefficients representing the crossed effects between fluxes and thermodynamic forces. It means that we will start with the balance equations for local variables, and then their closure will be written with linear relations and we will take into account all possible couplings, even the ones which are not usually taken for a simple fluid. The unusual transport coefficients will be proposed according to a dimensional analysis, the Onsager reciprocity principle, and the positiveness condition imposed on the entropy production. In Sec. II, the balance equations and the closure with constitutive relations are discussed. Section III is devoted to the Onsager symmetry between transport coefficients and in Sec. IV we calculate the entropy production in several particular cases. In Sec. V the set of equations to be solved is shown and some earlier results are synthesized. Section VI is devoted to the selection of parameter values according to the DSMC calculations and in Sec. VII all the LIT model results are given with the comparisons with experimental data and DSMC calculations. Last, in Sec. VIII we give some concluding remarks.

II. THE LINEAR IRREVERSIBLE THERMODYNAMIC APPROACH

In this section we will set the model to study the shock-wave structure, taking as a starting point the LIT approach [44]. This task will be done for a traveling wave which propagates with constant speed along one direction. In this case the variables describing the flow do not depend on the position coordinate ξ and time t separately; instead, they depend on the scaling variable $x = \xi - ct$, the quantity c is the constant traveling speed, and then the flow is self-similar in such a variable. It means that we can describe the flow in a reference frame which travels with constant speed along the propagation direction. From this point of view all variables in the flow seem to be frozen and in this reference frame the motion is steady and occurs between two equilibrium states [45,46]. In between, we can observe the shock-wave structure where all local variables depend on the scaling variable x, and then the speed $u(x)$, or density, as well as the temperature $T(x)$ change according to a steady one-directional motion. To start with the treatment, let us consider the balance equations for a simple fluid in a steady compressible flow regime characterized by the Mach number M, which is defined as the velocity of the shock wave at the part with lower temperature (the cold part of the shock) divided by the sound speed at this temperature. The mass balance across the shock wave implies that the mass flux is a fixed constant,

$$\rho(x)u(x) = C_1, \tag{1}$$

where $\rho(x)$ is the local mass density. In a similar way, the momentum balance drives us to write the momentum flux as a constant,

$$P_{xx}(x) + \rho(x)u(x)^2 = C_2, \quad P_{xx}(x) = p(x) + \sigma_{xx}(x), \tag{2}$$

where $P_{xx}(x)$ represents the pressure tensor which contains the local hydrostatic pressure $p(x)$ and $\sigma_{xx}(x)$ gives a measure of the corresponding viscous tensor. Also, the total energy balance plays a role by means of the energy flux which also remains constant, namely

$$\rho(x)u(x)\left[e(x) + \frac{P_{xx}(x)}{\rho(x)} + \frac{u(x)^2}{2}\right] + q(x) = C_3. \tag{3}$$

where $e(x)$, $q(x)$ are the specific internal energy and the heat flux, respectively.

In this case, the local equilibrium hypothesis will be taken for granted and this means that the hydrostatic pressure and the specific energy are written as functions of the independent variables which can be the density $\rho(x)$ and temperature $T(x)$; then $p(x) = p(\rho(x), T(x))$, and $e(x) = e(\rho(x), T(x))$ are taken from the local equation of state and the corresponding caloric equation. In this work we will consider a dilute monatomic ideal gas where the equation of state corresponds to the law of ideal gases and the internal energy is given in terms of energy equipartition for the three degrees of freedom in the gas, then

$$p(x) = \rho(x)\frac{k_B T(x)}{m}, \quad e(x) = \frac{3}{2}\frac{k_B T(x)}{m}, \tag{4}$$

where k_B is the Boltzmann constant and m the mass of particles.

The equilibrium points are obtained from Eqs. (1)–(3) when there are no dissipative fluxes in the system. It means that $\sigma_{xx}(x) = 0$, $q(x) = 0$ and all local quantities become constant. If we take the coordinates at up-flow (the cold part of the shock) to construct dimensionless variables as

$$v(x) = \frac{u(x)}{u_0}, \quad \tau(x) = \frac{k_B T(x)}{m u_0^2}, \tag{5}$$

where u_0 is the shock wave speed at up-flow where the velocity is supersonic, the Rankine-Hugoniot jump conditions, Eqs.(1)–(3), can be easily solved giving the two equilibrium

points coordinates:

$$P_0 = \left(1, \frac{3}{5M^2}\right) = (1, \tau_0),$$

$$P_1 = \left[\frac{3+M^2}{4M^2}, \frac{3(-3+14M^2+5M^4)}{80M^4}\right] = \left(\frac{1+5\tau_0}{4}, \frac{3}{16}+\frac{7}{8}\tau_0-\frac{5}{16}\tau_0^2\right), \quad (6)$$

which correspond to the up-flow and down-flow equilibrium points, respectively. Notice that the Mach number M is defined as the ratio between the shock speed (u_0) and the adiabatic speed of sound $c_0 = (\sqrt{5\,k_B\,T_0/3\,m})$, both calculated at up-flow.

To lead with this problem we will take the LIT approach to nonequilibrium problems in dilute gases [44,47], which has allowed us an approximate view of the gas behavior undergoing dissipative processes near equilibrium. This point of view gives a systematic way to consider a great variety of applications where linear constitutive equations are valid. We should note that the expression "near equilibrium" is a qualitatively assertion which has been extended to problems where the local equilibrium is far from been guaranteed. In particular, the shock-wave problem in dilute gases has been a challenge for a long time, mainly due to its intrinsic nature. Let us recall that the LIT scheme corresponds to a continuum description of phenomena and, in contrast, the shock wave represents almost a discontinuity in the flow (or at least very big changes of the relevant variables occurring in a narrow region). In this context, the usual NSF set of equations has been taken as a starting point to study the shock-wave structure. In a recent paper [1] we have taken the shear viscosity in a simple fluid as a power of the temperature with an index which enhances its effect. Moreover, such an index depends on the Mach number and it was adjusted with the normalized density profiles. No matter the success of this approach, we asked ourselves several questions about the physical mechanisms underlying the enhancement. In this section we will set a possible mechanism to achieve such an enhancement, starting with the phenomenological relation between the fluxes and the gradients. According to LIT, the dissipative fluxes follow linear relations with the position derivatives of the local variables $(u(x), T(x), \rho(x))$ through the transport coefficients which can be measured. It should be noted that we have taken the density as an independent variable, to be consistent with the physical view of a simple fluid in which there are usually two thermodynamic variables and the speed. This fact allows us to construct the fluxes $(\sigma_{xx}(x),\ q(x))$ in terms of the gradients of the local variables chosen, then

$$\sigma_{xx} = P_{xx} - p = b_1^*\frac{du}{dx} + b_2^*\frac{dT}{dx} + b_3^*\frac{d\rho}{dx}, \quad (7)$$

$$q = b_4^*\frac{du}{dx} + b_5^*\frac{dT}{dx} + b_6^*\frac{d\rho}{dx}, \quad (8)$$

where the coefficients $(b_1^*,\ b_2^*, \ldots, b_6^*)$ measure the intensity of the couplings between the gradients. It should be noted that the shock-wave mass conservation equation (1) tells us that the density and the speed are not independent; as a consequence, the density gradients in Eqs. (7) can be written in proportion to the speed derivative and it is not necessary to keep both. Actually, the term containing b_3^* gives rise to a gradient in the velocity that "renormalizes" the coefficient b_1^*, and a simliar argument can be given for the term containing $b_6^\star$, so that the enhancement of the viscosity used in a previous work can heuristically be understood in these terms. However, an atomistic approach is needed to support the enhancement and, as we will see, there are other mechanisms that can explain the experimental normalized density profiles without invoking the renormalization of the viscosity.

To follow the LIT structure we will take the Gibbs equation relating the changes in the specific entropy $s(x)$ with the heat transfer and the work done on the system. In fact, it assumes that the Gibbs $T\,ds$ equation is the same in terms of the local variables as it is in thermodynamic equilibrium. In our case we have

$$\frac{\partial \rho s}{\partial t} + \frac{\partial}{\partial x}\left(\rho s u + \frac{1}{T}q_x\right) = q_x\frac{\partial T}{\partial x} - \frac{1}{T}\sigma_{xx}\frac{\partial u}{\partial x}, \quad (9)$$

where the right-hand side is identified with the specific entropy production

$$\Sigma_s(x) = q_x(x)\frac{\partial}{\partial x}\left[\frac{1}{T(x)}\right] - \frac{1}{T(x)}\sigma_{xx}(x)\frac{\partial u(x)}{\partial x}. \quad (10)$$

Hence, we will define the usual fluxes and thermodynamic forces as follows:

$$J_{\sigma,q} = [\sigma_{xx},\ q_x], \quad X_{\sigma,q} = \left[-\frac{1}{T}\frac{du}{dx},\ \frac{d}{dx}\left(\frac{1}{T}\right)\right], \quad (11)$$

and the linear relation between fluxes and thermodynamic forces is then written in the following way:

$$\sigma_{xx}(x) = L_{\sigma\sigma}X_\sigma(x) + L_{\sigma q}X_q(x), \quad (12)$$

$$q(x) = L_{q\sigma}X_\sigma(x) + L_{qq}X_q(x), \quad (13)$$

where the transport coefficients L_{ij}, which in fact are related with the b^*s written in Eq. (7), can be some functions of the position coordinates through the variables in the system.

A direct dimensional analysis in terms of $(\eta,\ T)$ allows us to write

$$L_{\sigma\sigma} = -a_1\eta T, \quad L_{\sigma q} = -a_2\eta T\sqrt{\frac{k_BT}{m}}, \quad (14)$$

$$L_{q\sigma} = -a_3\eta T\sqrt{\frac{k_BT}{m}}, \quad L_{qq} = -a_4\eta\frac{k_BT^2}{m}, \quad (15)$$

where η is the viscosity and the quantities $(a_1,\ a_2,\ a_3,\ a_4)$ are dimensionless functions of all combinations of dimensionless variables and parameters in the problem. Their values will be chosen and discussed below.

III. THE ONSAGER SYMMETRY

Up to this point the LIT scheme has been followed in a direct way. However, we have considered the crossed effects between the viscous tensor and the heat flux with both thermodynamic forces present in the system. In the usual LIT scheme, the Curie principle is taken for granted with the idea of full isotropy in fluxes and forces, as is usual near

equilibrium processes in a monatomic gas. As we stated, we think that the shock-wave problem is somewhat special due to the fact that there are very large changes in the relevant variables (speed, temperature, and density) and those changes occur in a very narrow region. Moreover, such a steep change occurs in the shock-wave propagation direction, provoking an anisotropic situation along such a direction and its transversal plane. This fact indicates that the usual isotropic hypothesis basic for the Curie's principle to be applied may be not completely valid. In particular, the constitutive equations give us the opportunity to prove other schemes based on such lack of isotropy. In this sense we are assuming that the crossed effects are present in the shock-wave structure.

In fact, there are some indications about this lack of isotropy as noticed by Hoover, Holian, and some other authors [41,48,49], where they introduced explicitly the longitudinal temperature in a one-directional shock wave that is clearly defined, and it is different from the transversal one, as will be shown in Sec. VII. Also, it is important to recall that the thermal transpiration effect is present in a rarefied gas when there are large changes in the temperature and a wall is present and then a motion appears. In our model, the motion produced by a temperature gradient is measured with the $L_{\sigma q}$ coefficient. On the other hand, the coefficient $L_{q\sigma}$ becomes its conjugate, producing a heat flow as a consequence of the speed gradient.

The problem we face now is the selection of values for these coefficients going beyond the dimensional analysis, as we have stated above. At first glance, we will ask them to satisfy the Onsager symmetry relation, though it is not necessary, as argued by Coleman-Truesdell [50].

Even then, we will assume the Onsager symmetry is valid and write the relation between crossed coefficients following the rules given in the literature [44]. To do such a task we note that the concerned variables, temperature and speed, have different properties when time inversion is done [47]. This means that the Onsager symmetry must take into account this fact, and then

$$L_{ij} = \epsilon_i \epsilon_j L_{ji}, \tag{16}$$

where $\epsilon_i,\ \epsilon_j$ become (± 1) according to the parity properties. This means that

$$L_{\sigma q} = -L_{q\sigma}. \tag{17}$$

Going back to Eqs. (14) this condition means that the dimensionless quantities $(a_2,\ a_3)$ must satisfy the condition $a_3 = -a_2$. Finally, the proposed constitutive equations are written as

$$\sigma_{xx} = a_1 \eta \frac{du}{dx} + a_2 \frac{\eta}{T}\sqrt{\frac{k_B T}{m}}\frac{dT}{dx}, \tag{18}$$

$$q_x = -a_2 \eta \sqrt{\frac{k_B T}{m}}\frac{du}{dx} + a_4 \eta \frac{k_B}{m}\frac{dT}{dx}. \tag{19}$$

The selection for the set of quantites $(a's)$ will generate different models which follow the LIT scheme, and then the comparison of numerical results coming from the LIT model with the experimental data will play a crucial role.

Last, the shear viscosity is given as follows:

$$\eta = \eta_0 \left(\frac{\tau}{\tau_0}\right)^{\sigma}. \tag{20}$$

IV. THE ENTROPY PRODUCTION

The usual framework in LIT tells us that the entropy production (Σ_s) is given as a product of the fluxes and their corresponding thermodynamic forces; in our case the identification is given in Eq. (11), so

$$\Sigma_s(x) = \sum_i J_i X_i, \tag{21}$$

where the sum is done over all pair flux-force in the process. Now the entropy production is immediately constructed,

$$\Sigma_s(x) = L_{\sigma\sigma} X_\sigma^2 + L_{qq} X_q^2 + (L_{\sigma q} + L_{q\sigma}) X_\sigma X_q, \tag{22}$$

which is a bilinear form in the thermodynamic forces.

Then, with the direct substitution of Eqs. (18) in the entropy production, we obtain that

$$\Sigma_s = -a_1 \eta T X_\sigma^2 - a_4 \eta \frac{k_B T^2}{m} X_q^2 + (a_2 + a_3)\eta T \sqrt{\frac{k_B T}{m}} X_\sigma X_q, \tag{23}$$

where we must ask that the quadratic form be positive definite, a condition which impose a limitation to the coefficients values, namely

$$a_1 \leqslant 0, \tag{24}$$

$$a_4 \leqslant 0, \tag{25}$$

$$a_1 a_4 - \frac{(a_2 + a_3)^2}{4}\frac{mu(x)^2}{k_B T(x)} \geqslant 0. \tag{26}$$

It should be recalled that, in the general case, the a coefficients are undetermined functions of the Mach number M and the dimensionless variables we are dealing with. Now it is interesting to consider some particular cases and begin the model analysis.

A. The Navier-Stokes-Fourier regime

The usual NSF equations can be obtained with the selection for the a coefficients: $(a_1 = -4/3,\ a_4 = -15/4,\ a_2 = a_3 = 0)$, then the entropy production is written as

$$\Sigma_{\rm NS} = \frac{4\eta}{3}\left[\frac{du(x)}{dx}\right]^2 + \frac{15\eta k_B}{4m}\left[\frac{dT(x)}{dx}\right]^2, \tag{27}$$

where it is clear that $\Sigma_{\rm NS} \geqslant 0$, as asked in LIT, when the viscosity is positive, see Eq. (20). Here the ratio between the coefficients drives us to the the usual relation for the viscosity and the thermal conductivity in a dilute monatomic gas, no matter the temperature or the Mach number dependence in the viscosity, as was considered recently [1].

B. The LIT model

The generalization proposed in this paper corresponds to the coupling between the viscous tensor and the heat flux through the coefficients a_2, a_3. In such a case the coupling between fluxes and forces is responsible for a new term in the entropy production, as shown in Eq. (23). However, when the Onsager relations are taken into account (see Sec. III), the entropy production simplifies,

$$\Sigma_s = -a_1\eta X_\sigma^2 - a_4\eta\frac{k_B T^2}{m}X_q^2, \tag{28}$$

an expression with the same structure as in the NSF case. However, it is really important to keep in mind that the variables v, τ satisfy a different set of equations as will be set explicitly in the next section. Then the functions (v, τ) are not the same as in the NSF model.

V. THE SHOCK-WAVE STRUCTURE IN THE LIT MODEL

To go further, let us write the set of equations based on the thermodynamic approach; the proposed constitutive relations are written as follows:

$$\sigma_{xx} = \frac{\eta\, u_0}{\lambda}\left(a_1\frac{dv}{ds} + a_2\tau^{1/2}\frac{d\tau}{ds}\right), \tag{29}$$

$$q_x = \frac{\eta\, u_0^2}{\lambda}\left(a_3\tau^{1/2}\frac{dv}{ds} + a_4\frac{d\tau}{ds}\right), \tag{30}$$

where s is the reduced distance,

$$s = \frac{x}{\lambda}. \tag{31}$$

Several elections for λ are used in the literature. In the experiments the value used for λ is Alsmeyer's mean free path (λ_A) defined as,

$$\lambda_A \equiv \frac{16}{5}\sqrt{\frac{5}{6\pi}}\frac{\eta_0}{\rho_0 a_0}, \tag{32}$$

where $a_0 = \sqrt{5k_BT_0/3m}$ is the argon speed of sound at up-flow. In this work we use this Alsmeyer's mean free path and

$$\lambda_2 \equiv \frac{4}{3}\frac{\eta_0}{\rho_0\, u_0} \tag{33}$$

to reduce the distance as in a previous work [1]. The results of solving the differential equations that appear below—see Eqs. (36)—using for λ the values λ_A and λ_2 were done independently and the numerical outputs of both were compared as a test for accuracy. In this work we report our results in terms of Alsmeyer's reduced distance s_A defined by

$$s_A = \frac{x}{\lambda_A}, \tag{34}$$

where x is the distance along the shock, the origin is taken as the point at which the normalized density profile has the value $1/2$ and λ_A is Alsmeyer's mean free path given by Eq. (32).

Moreover, we have assumed a soft-sphere temperature dependence in the shear viscosity, hence

$$\eta = \eta_0\left[\frac{\tau(s)}{\tau_0}\right]^\sigma, \tag{35}$$

and the σ index will be taken with a fixed value for each Mach number; however, it will not be the only quantity to be adjusted in the model, as we reported in Ref. [1].

The direct substitution of Eqs. (29) and (30) in the conservation equations (1), (2), and (3) expressed in terms of the dimensionless variables drives us to

$$a_1\frac{dv}{ds} + a_2\tau(s)^{1/2}\frac{d\tau}{ds} = \frac{\rho_0 u_0\lambda}{\eta}\left(1 + \tau_0 - \frac{\tau}{v} - v\right), \tag{36a}$$

$$(a_1 v + a_3\tau^{1/2})\frac{dv}{ds} + (a_4 + a_2 v\tau^{1/2})\frac{d\tau}{ds} = \frac{\rho_0 u_0\lambda}{2\eta}(5\tau_0 + 1 - 5\tau - v^2). \tag{36b}$$

Notice that in

$$\frac{\rho_0 u_0\lambda_A}{\eta_0} = \frac{16}{5}\sqrt{\frac{5}{6\pi}}M \quad \text{and} \quad \frac{\rho_0 u_0\lambda_2}{\eta_0} = \frac{4}{3}, \tag{37}$$

all quantities with subscript "0" are calculated at up-flow. In this work we will choose the simplest selection for the values in the as; in particular $\sigma(M)$, $a_1 = -4/3$, $a_4 = -15/4$ in the NSF case and $a_2(M) = -a_3(M)$ to satisfy the Onsager relation. Then, we have at most two adjustable parameters for each Mach number, namely $(\sigma,\ a_2)$. From Eqs. (36) we can solve for the derivatives with the result that

$$\frac{dv}{ds} = \frac{\rho_0\, u_0\,\lambda}{2\,\eta}\,\frac{[3\,\tau\, - v^2 + 2\,v(\tau_0+1) - \ (1+5\,\tau_0)](v\,\sqrt{\tau}\,a_2) + 2\,[-\,v^2 + \ v(\tau_0+1) - \ \tau\,]\,a_4}{(a_1\,a_4 - \tau\,a_2\,a_3)v}, \tag{38a}$$

$$\frac{d\tau}{ds} = \frac{\rho_0\, u_0\,\lambda}{2\,\eta}\,\frac{[3\,\tau\, - v^2 + 2\,v(\tau_0+1) - \ (1+5\,\tau_0)](-v\,a_1) + 2\,[-\,v^2 + \ v(\tau_0+1) - \ \tau](-\sqrt{\tau}\,a_3)}{(a_1\,a_4 - \tau\,a_2\,a_3)v}. \tag{38b}$$

It should be pointed out that in going from the implicit set of equations of the derivatives to the explicit ones, singularities can appear since $\Xi \equiv a_1\,a_4 - \tau\,a_2\,a_3$ can be zero. If a_1 and a_4 are negative, then the reciprocity condition $a_3 = -a_2$ implies that Ξ is always positive because τ is always non-negative and, consequently, there are no singularities for the derivatives. For a study of the implications of the existence of singularities for the Maxwell-Cattaneo model, see Ref. [27].

The NSF hydrodynamic model is obtained by using $a_1 = -4/3$, $a_2 = -a_3 = 0$, and $a_4 = -15/4$ in Eqs. (38).

Now let us set the different alternatives. The first step was done through the study of the NSF model as reported recently [1]. In this case we have found the following:

(1) The orbit in the plane $(v,\ \tau)$ determined by the model equations does not depend on the viscosity index proposed. Its agreement with DSMC calculations is good for $M = 1.2$,

but it is far from reasonable for $M = 8.0$, even in a qualitative comparison, as shown in Ref. [1] (see Fig. 3).

(2) The normalized density profile can be adjusted with a viscosity index $\sigma(M)$, giving a remarkable result when the model is compared with DSMC calculations or experimental data [20]. However, it is important to notice that such an index has a value larger than the one reported by some authors to reproduce the measurements of the viscosity [32]. But, as we will see, for DSMC the values of σ that better fit the experimental normalized density profiles are higher than those recommended in the literature [51,52]; in other words, an enhancement of the viscosity is needed to fit the experimental density profiles for the NSF model [1] and DSMC.

(3) The normalized temperature profile does not show good results when compared with DSMC.

(4) The reciprocal shock thickness as well as the asymmetry factor agree qualitatively with reported results.

It is important to recall that the main conclusion in the NSF model is the need of an enhancement in the viscosity, as represented by the index $\sigma(M)$, to give a good agreement with the normalized density profiles. In such a context we ask ourselves if there are some other alternatives to reproduce the normalized dentiy profiles; in fact, this was our motivation to undertake this work. The LIT model we have constructed offers us the opportunity to achieve such a task. Now we will study some consequences of the new hypotheses.

First, we must be aware of the fact that the orbit equation in the LIT model does not depend on the viscosity or λ as it is shown by calculating $d\tau/dv$ from Eqs. (38). It means that the NSF as well as the LIT model are independent of the interaction potential between particles.

To go further in the orbit calculation, we must give the possible values for $a_2(M)$ and, to calculate the density and temperature profiles, both parameters $[a_2(M), \sigma(M)]$ must be chosen. This means that we need a criterion to choose

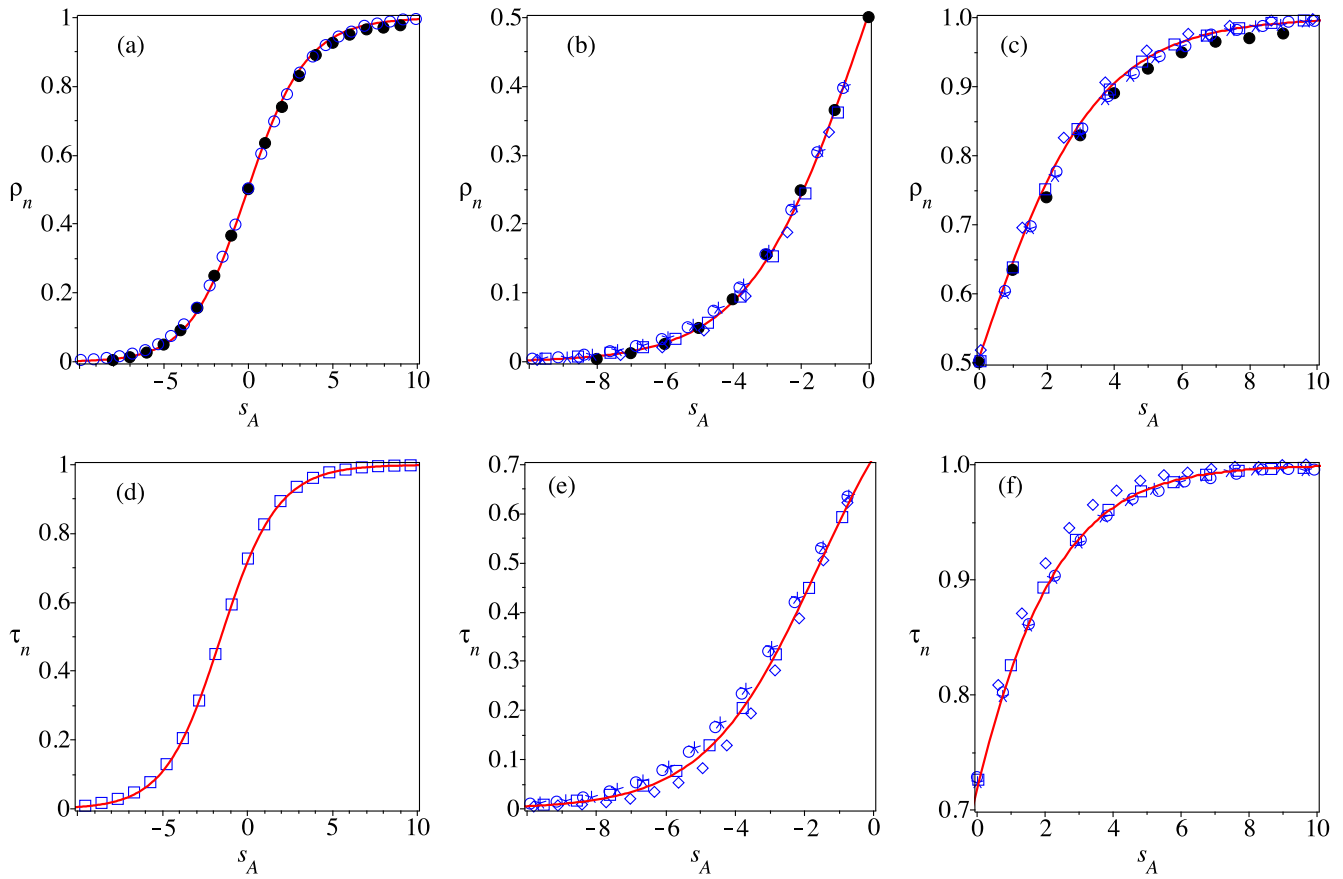

FIG. 1. Normalized density and temperature profiles for argon at $M = 1.55$. (a) Normalized density profiles vs Almeyer's reduced distance, ρ_n vs s_A. Solid circles: Experiments by Alsmeyer [20]; open circles: Bird's DSMC for $\sigma = 1.2$ and $\alpha^{-1} = 0.6525$; solid line: DSMC by Sharipov and Dias [55] at $M = 1.5$. (b) Normalized density profiles vs Almeyer's reduced distance, ρ_n vs s_A. Solid circles: Experiments by Alsmeyer [20]; open circles: Bird's DSMC for $\sigma = 1.2$ and $\alpha^{-1} = 0.6525$; asterisks: Bird's DSMC for $\sigma = 1.2$ and $\alpha = 1$; diamonds: Bird's DSMC for $\sigma = 1.0$ and $\alpha^{-1} = 0.6525$; boxes: Bird's DSMC for $\sigma = 1.0$ and $\alpha^{-1} = 0.6525$; solid line: DSMC by Sharipov and Dias [55] at $M = 1.5$. (c) Normalized density profiles vs Almeyer's reduced distance, ρ_n vs s_A. Legend as in (b). (d) Normalized temperature profiles vs Almeyer's reduced distance, τ_n vs s_A. Boxes: Bird's DSMC for $\sigma = 1.0$ and $\alpha^{-1} = 0.6525$; solid line: DSMC by Sharipov and Dias [55] at $M = 1.5$. (e) Normalized temperature profiles vs Almeyer's reduced distance, τ_n vs s_A. Open circles: Bird's DSMC for $\sigma = 1.2$; asterisks: Bird's DSMC for $\sigma = 1.2$ and $\alpha = 1$; diamonds: Bird's DSMC for for $\sigma = 1.0$ and $\alpha^{-1} = 0.6525$; boxes: Bird's DSMC for $\sigma = 1.0$ and $\alpha^{-1} = 0.6525$; solid line: DSMC by Sharipov and Dias [55] at $M = 1.5$. (f) Normalized temperature profiles vs Almeyer's reduced distance, τ_n vs s_A. Legend as in (e).

them even in the simplest case when we consider that they only depend on the Mach number M. Such a criterion will be done by the best fit with the experimental normalized density profiles and the orbits given by the DSMC method as we discuss below.

We summarize the models that will be considered in this work as follows:

(i) The NSF model, studied previously [1], consists of using the NSF constitutive equations to solve the shock-wave problem. The viscosity-temperature index σ is adjusted to reproduce the normalized density profiles for each Mach number. This is a one-parameter model.

(ii) The one-parameter LIT model, LIT1, consists of taking $a_1 = -4/3$, $a_2 = -a_3$, and $a_4 = -15/4$. The viscosity-temperature index σ is chosen to reproduce the experimental values for the viscosity and a_2 is adjusted to reproduce the experimental values of the normalized density profiles for each Mach number. Hence, there is no enhancement of the viscosity and the experimental normalized density profiles are fit by adjusting a_2.

(iii) A two-parameter LIT model, LIT2, is obtained by taking $a_1 = -4/3$, $a_2 = -a_3$, and $a_4 = -15/4$. The index σ as well as a_2 are adjusted to reproduce the experimental normalized density profiles and the orbits predicted by DSMC for each Mach number.

VI. THE DIRECT SIMULATION MONTE CARLO METHOD

Experimental information on shock waves is scarce but, fortunately, with the advent of the computer, more data can be obtained through simulations. The Monte Carlo method [53], MD [48], and the DSMC method [51,52] are some examples. For dilute gases the well-established Boltzmann equation provides a sound atomistic theory from which several results can be obtained, sometimes with a lot of effort, when model or realistic interaction potentials are given [2].

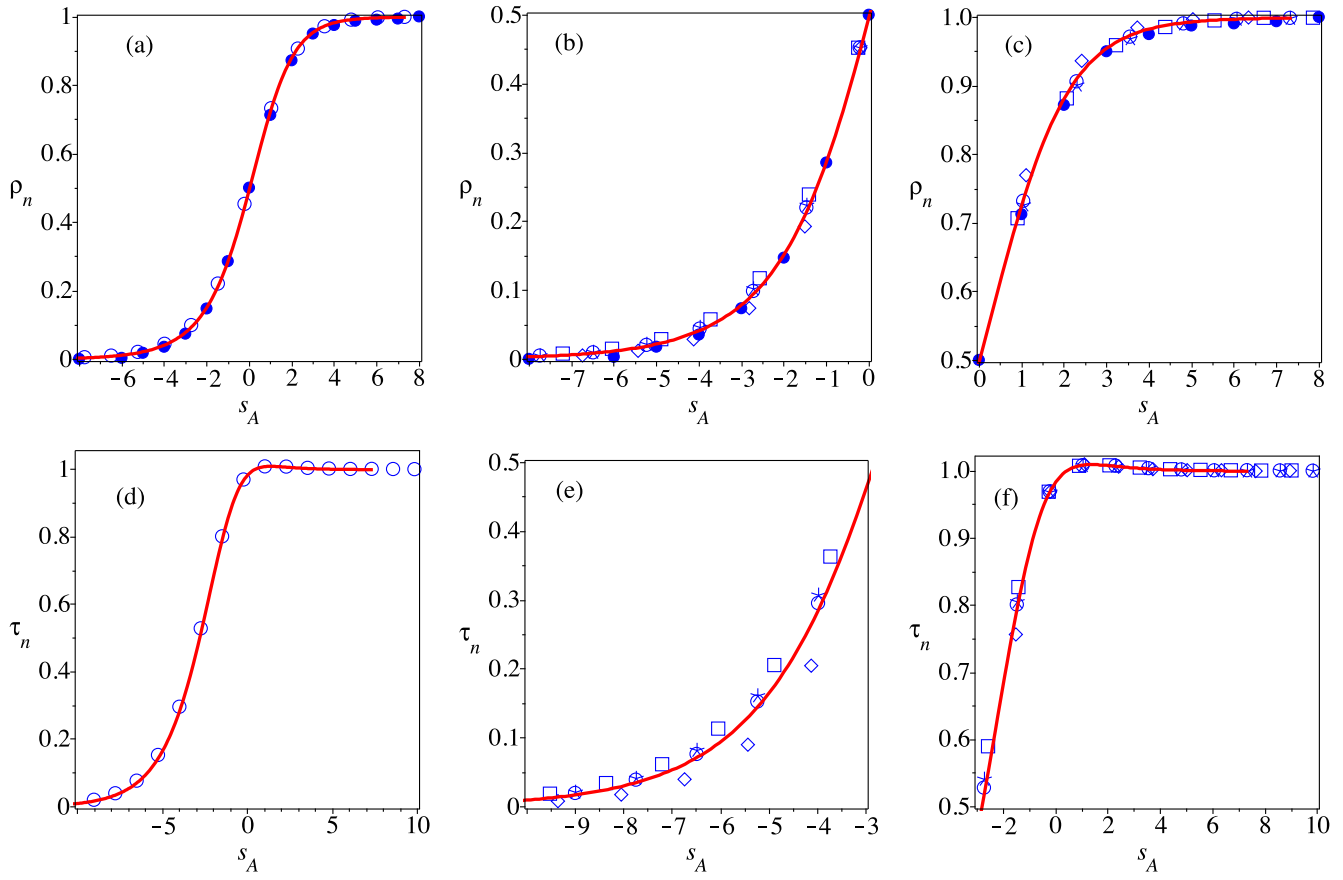

FIG. 2. Normalized density and temperature profiles for argon at $M = 9$. (a) Normalized density profiles vs Almeyer's reduced distance, ρ_n vs s_A. Solid circles: Experiments by Alsmeyer [20]; open circles: Bird's DSMC for $\sigma = 0.72$ and $\alpha^{-1} = 0.6015$; solid line: DSMC by Sharipov and Dias [55] for $M = 10$. (b) Normalized density profiles vs Almeyer's reduced distance, ρ_n vs s_A. Solid circles: Experiments by Alsmeyer [20]; open circles: Bird's DSMC for $\sigma = 0.72$ and $\alpha^{-1} = 0.6015$; asterisks: Bird's DSMC for $\sigma = 0.72$ and $\alpha = 1$; diamonds: Bird's DSMC for $\sigma = 0.68$ and $\alpha^{-1} = 0.6525$; boxes: Bird's DSMC for $\sigma = 0.81$ and $\alpha^{-1} = 0.6525$; solid line: DSMC by Sharipov and Dias [55] for $M = 10$. (c) Normalized density profiles vs Almeyer's reduced distance, ρ_n vs s_A. Legend as in (b). (d) Normalized temperature profiles vs Almeyer's reduced distance, τ_n vs s_A. Open circles: Bird's DSMC for $\sigma = 0.72$ and $\alpha^{-1} = 0.6015$; solid line: DSMC by Sharipov and Dias [55] for $M = 10$. (e) Normalized temperature profiles vs Almeyer's reduced distance, τ_n vs s_A. Open circles: Bird's DSMC for $\sigma = 0.72$ and $\alpha^{-1} = 0.6015$; asterisks: Bird's DSMC for $\sigma = 0.72$ and $\alpha^{-1} = 1.0$; diamonds: Bird's DSMC for $\sigma = 0.68$ and $\alpha^{-1} = 0.6525$; boxes: Bird's DSMC for $\sigma = 0.81$ and $\alpha^{-1} = 0.6525$; solid line: DSMC by Sharipov and Dias [55] for $M = 10$. (f) Normalized temperature profiles vs Almeyer's reduced distance, τ_n vs s_A. Legend as in (e).

In 1992 Wagner [54] was able to show that Bird's implementation of the DSMC method can actually be regarded as a probabilistic solution to the Boltzmann equation. Nowdays, this method is the one that is usually used by researches for dilute gases, although MD, the method of choice for dense gases, liquids, or solids, has also been used and comparisons with DSMC are available [49].

A point that must be addressed is the following: What is interatomic interaction potential? Usually the methods that are more appealing are those based on first principles, called *ab initio*, although model potentials will be used in this work. Therefore, we first compare results coming from *ab initio* interatomic potentials and model potentials and determine the model potentials that better fit the experimental data.

The model potentials that we will consider are those mentioned by Bird [51,52], the variable hard-sphere (VHS) and the variable soft-sphere (VSS) models. The first one (VHS) was introduced by Bird in 1981 [51] in order to obtain a finite total cross section using a diameter d that is a function of the relative velocity, c_r, in a binary collision,

$$d \propto c_r^{-\vartheta}, \tag{39}$$

where $\vartheta = \sigma - 1/2$ and σ is such that the model gives a viscosity proportional to T^{σ}, where T is the temperature. We will refer to σ as the temperature–viscosity index. For this model the deflection angle is given by

$$\chi = 2\cos^{-1}(b/d), \tag{40}$$

where b is the impact parameter. Bird pointed out [52] that the VHS model does not provide a correct Schmidt number—it is defined as the shear viscosity divided by the product of the density and the self-diffusion coefficient— for flows dominated by diffusion so that in order to fix this point it is better to introduce the VSS model in which, instead of Eq. (40), one has

$$\chi = 2\cos^{-1}[(b/d)^{1/\alpha}], \tag{41}$$

where α is chosen to match the Schmidt number. Most of our DSMC computations use the VSS model. For argon Bird recommends the values $\sigma = 0.81$ and $\alpha = 1.4$ [51]; we will consider σ as an adjustable parameter and take, in most cases, $\alpha = 1.53$, where the value of α does not affect the shock-wave profiles in a sensible way.

Recently, Sharipov and Dias [55] used *ab initio* data to calculate planar shock-wave profiles for helium, neon, and argon using the DSMC method. They commented that the computations times are about the same as the model potentials discussed above and that their computations are free from the adjustable parameters of such model potentials, σ, for example. As they pointed out, the *ab initio* information is usually provided in tables and it is necessary to find an interpolating formula for such data; for example, in the method of classical trajectories the relevant cross sections needed to calculate the transport coefficients, among other physical quantities, are obtained using an interpolating formula to fit the *ab initio* information in order to obtain the interaction potential. Leaving aside that there can be several interpolating forms, it should be pointed out that their interpolating function for argon has 14 interpolating coefficients that have to be determined. Another important point is access, not to mention simplicity; we do not know where their program can be obtained, but Bird's program for shock waves is accessible [51]. Previously, Sharipov and Strapasson [56] considered the Lennard-Jones potential and claimed that their scheme dispenses the model potentials mentioned above. Bird's comment on this was as follows [52]: *A model with a greater degree of physical realism does not necessarily lead to a more accurate result*. For a detailed discussion on this point, see Sec. 3.1 in Ref. [52]. Further comments on the DSMC method are given in Appendix.

We now proceed to make a comparison of the DSMC method using model and *ab initio* potentials, but first we note that Sharipov and Dias reduced the position with their "mean free path" that is given by

$$\lambda_S \equiv \sqrt{\frac{2\,k_B\,T}{m}}\,\frac{\eta}{p}, \tag{42}$$

while Bird's mean free path is

$$\lambda_B \equiv \frac{4\,\alpha\,(5-2\,\sigma)\,(7-2\,\sigma)}{5\,\pi^2\,(\alpha+1)\,(\alpha+2)}\,\sqrt{\frac{m}{2\,k_B\,T}}\,\frac{\eta}{\rho}. \tag{43}$$

Furthermore, the experimental data for the normalized density are expressed in terms of the reduced distance by Alsmeyer's "mean free path" defined by Eq. (32),

$$\lambda_A \equiv \frac{16}{5}\,\sqrt{\frac{\gamma}{2\,\pi}}\,\frac{\eta}{\rho\,a}, \tag{44}$$

where γ is the specific heat ratio and a is the velocity of sound.

TABLE I. Results for the asymmetry factor and the reciprocal width for several Mach numbers. The quantities with an E superiscript come from the experimental data.

Model	M	σ	a_2	α^{-1}	$\overline{Q}_\rho$	$\overline{Q}_\rho^E$ [20]	λ_A/δ	λ_A/δ^E [20]
NSF	1.55	1.6	0.0	*NA*	1.00	0.92	0.13	0.12
DSMC	1.55	1.2	*NA*	0.6525	0.96	0.92	0.15	0.12
LIT1	1.55	0.72	−1.75	*NA*	1.12	0.92	0.14	0.12
LIT2	1.55	1.5	−0.25	*NA*	1.03	0.92	0.13	0.12
NSF	2.05	1.3	0	*NA*	1.08	0.96	0.20	0.21
DSMC	2.00	0.81	*NA*	0.6525	0.99	0.96	0.20	0.21
LIT1	2.05	0.72	−2.5	*NA*	1.16	0.96	0.20	0.21
LIT2	2.05	0.9	−1	*NA*	1.19	0.96	0.22	0.21
NSF	3.38	1.05	0.0	*NA*	1.18	1.02	0.28	0.28
DSMC	3.38	0.75	*NA*	0.6525	1.10	1.02	0.28	0.28
LIT1	3.38	0.72	−2.5	*NA*	1.29	1.02	0.29	0.28
LIT2	3.38	0.9	−1.0	*NA*	1.28	1.02	0.29	0.28
NSF	6.5	1.05	0.0	*NA*	1.20	1.12	0.20	0.25
DSMC	6.5	0.72	*NA*	0.6015	1.13	1.12	0.26	0.25
LIT1	6.5	0.76	−2.5	*NA*	1.35	1.12	0.26	0.25
LIT2	6.5	0.82	−1.5	*NA*	1.36	1.12	0.27	0.25
NSF	8.0	0.9	0.0	*NA*	1.28	1.13	0.26	0.24
DSMC	8.0	0.68	*NA*	0.6015	1.14	1.13	0.26	0.24
LIT1	8.0	0.76	−2.0	*NA*	1.38	1.13	0.27	0.24
LIT2	8.0	0.80	−1.5	*NA*	1.37	1.13	0.27	0.24
NSF	9.0	0.9	0.0	*NA*	1.26	1.14	0.24	0.23
DSMC	9.0	0.72	*NA*	0.6015	1.15	1.14	0.23	0.23
LIT1	9.0	0.76	−2.0	*NA*	1.38	1.14	0.26	0.23
LIT2	9.0	0.8	−1.5	*NA*	1.37	1.14	0.25	0.23

From the previous equations it follows that for a monatomic gas we have

$$\lambda_S = \frac{5}{8}\sqrt{\pi}\,\lambda_A \quad \text{and} \quad \lambda_A = \frac{4\,(\alpha+1)\,(\alpha+2)}{\alpha\,(2\,\sigma-7)\,(2\,\sigma-5)}\,\lambda_B, \quad (45)$$

and such relations are used to relate the different results from experiments and the two DSMC computations. The mean free paths are evaluated at the cold part of the shock.

The normalized density and temperature profiles, see Eq. (46) for their definition, for argon are given in Fig. 1 for $M = 1.55$. The normalized density profiles are shown in Fig. 1(a), and good agreement with the experimental values by Alsmeyer [20] is apparent for both Bird's DSMC for $\sigma = 1.2$ and $\alpha^{-1} = 0.6525$ and the DSMC *ab initio* computations by Sharipov and Dias [55]. In Figs. 1(b) and 1(c), a closer look at the comparison is shown and in addition three other computations for Bird's DSMC for different model potentials are also given. We notice that Sharipov and Dias's computations are closer to the experimental values by Alsmeyer for $s_A < 0$ than Bird's DSMC, for $\sigma = 1.2$ and $\alpha^{-1} = 0.6525$, but the opposite holds for $s_A > 0$. Also, we conclude that the VSS model potential that best represents the values by Sharipov and Dias corresponds to $\sigma = 1.0$ (Maxwell model) and $\alpha^{-1} = 0.6525$ and the VSS model that gives better agreement with the experimental data corresponds to $\sigma = 1.2$ and $\alpha^{-1} = 0.6525$. Notice that the VHS model ($\alpha = 1$) for $\sigma = 1.2$ gives practically the same values as the VSS model with the same value of σ. Finally, computations with the value for the VHS potential recommended by Bird [51] for argon ($\sigma = 0.81$) is also considered. Based on the agreement with the experimental data we will use the VSS model potential with $\sigma = 1.2$ and $\alpha^{-1} = 0.6525$ to make further comparisons such as the normalized temperature density profiles that are shown in Figs. 1(d)–1(f). Actually, such way of proceeding, adjusting the value of σ for the DSMC computations to fit the experimental data, was suggested in

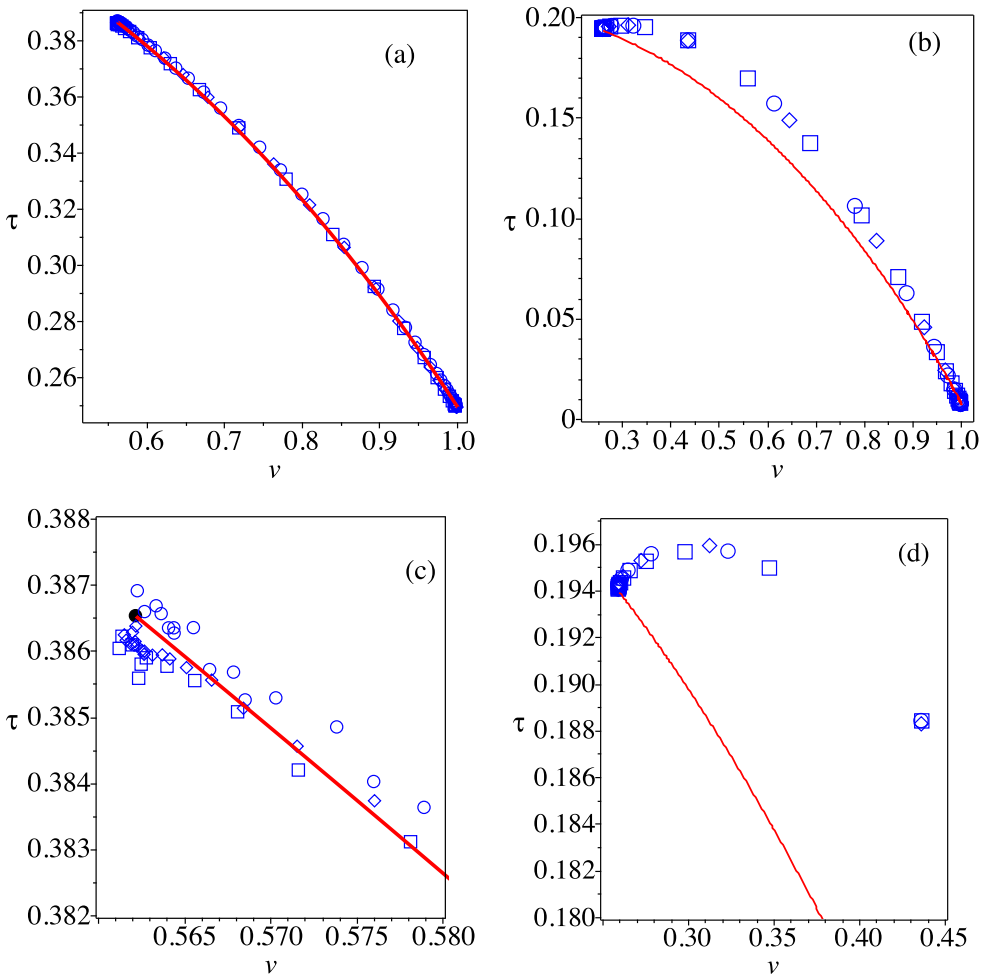

FIG. 3. Reduced temperature vs reduced velocity; τ vs v for argon for different Mach numbers. (a) τ vs v for argon at $M = 1.55$. open circles: Bird's DSMC for $\sigma = 1.2$ and $\alpha^{-1} = 0.6525$; diamonds: Bird's DSMC for $\sigma = 1.0$ and $\alpha^{-1} = 0.6525$; boxes: Bird's DSMC for $\sigma = 1.0$ and $\alpha^{-1} = 0.6525$; solid line: NSF hydrodynamic model [1]. (b) τ vs v for argon at $M = 9$. open circles: Bird's DSMC for $\sigma = 0.72$ and $\alpha^{-1} = 0.6015$; diamonds: Bird's DSMC for $\sigma = 0.68$ and $\alpha^{-1} = 0.6525$; boxes: Bird's DSMC for $\sigma = 0.81$ and $\alpha^{-1} = 0.6525$; solid line: NSF hydrodynamic model [1]. (c) τ vs v for argon at $M = 1.55$. open circles: Bird's DSMC for $\sigma = 1.2$ and $\alpha^{-1} = 0.6525$; diamonds: Bird's DSMC for $\sigma = 1.0$ and $\alpha^{-1} = 0.6525$; Solid circle: Down-flow (hot part of the shock wave); solid line: NSF hydrodynamic model [1]. (d) τ vs v for argon at $M = 9$. Open circles: Bird's DSMC for $\sigma = 0.72$ and $\alpha^{-1} = 0.6015$; diamonds: Bird's DSMC for $\sigma = 0.68$ and $\alpha^{-1} = 0.6525$; boxes: Bird's DSMC for $\sigma = 0.81$ and $\alpha^{-1} = 0.6525$; solid line: NSF hydrodynamic model [1].

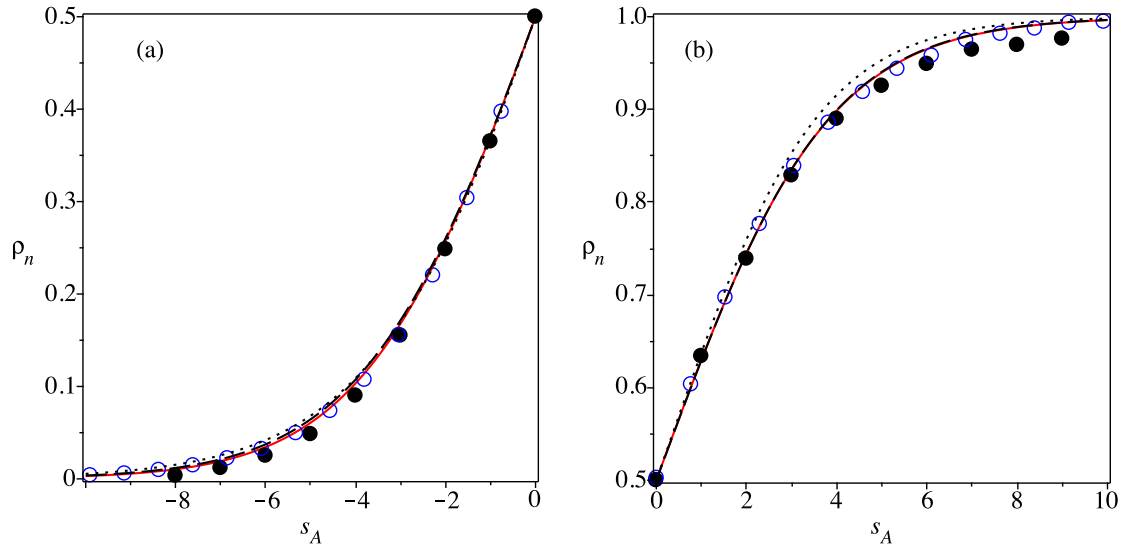

FIG. 4. Normalized density profiles, ρ_n vs s_A, for $M = 1.55$ in two different regions [(a) and (b)]. Solid circles: Experiments [20]; open circles: DSMC for $\sigma = 1.2$ and $\alpha^{-1} = 0.6525$; solid line: NSF; dashed line: LIT2; dotted line: LIT1, where the values for a_2 and σ are given in Table I.

a previous work by us [1] and here we fill this gap, and the values of σ that give a better agreement with the experimental information for the VSS model potentials at different Mach numbers are given in Table I. With respect to the temperature profiles shown in Figs. 1(d)–1(f), we note that the differences between the model potentials are more notorious than those in the normalized density profiles; as we mentioned above the model potential that better reproduces the *ab initio* DSMC normalized density profiles computations corresponds to the Maxwell model ($\sigma = 1$) and it also provides very good agreement with the *ab initio* DSMC normalized temperature profiles, as is shown in Figs. 3(b) and 3(c).

In order to see if our conclusions made for $M = 1.55$ hold for larger Mach numbers we provide a similar comparison for $M = 9$ in Fig 2. In this case the value of the viscosity-temperature index that provides good agreement with the experimental information on the normalized density profiles by Alsmeyer is $\sigma = 0.72$ with $\alpha^{-1} = 0.6015$, see Fig. 2(a). The value of α is not very important and the VHS model ($\alpha = 1$) provides also very good agreement. While there are differences between the VSS model and the *ab initio* DSMC the results are practically equivalent, and this is illustrated in Figs. 2(b) and 2(c). Notice that the *ab initio* DSMC computations are for $M = 10$ while all others are for $M = 9$. In Figs. 2(a)–2(c) we also provide other VSS model potentials to see the effect of the viscosity-temperature index. As for the case $M = 1.55$, there is a more noticeable difference in the normalized temperature profiles than in those of the

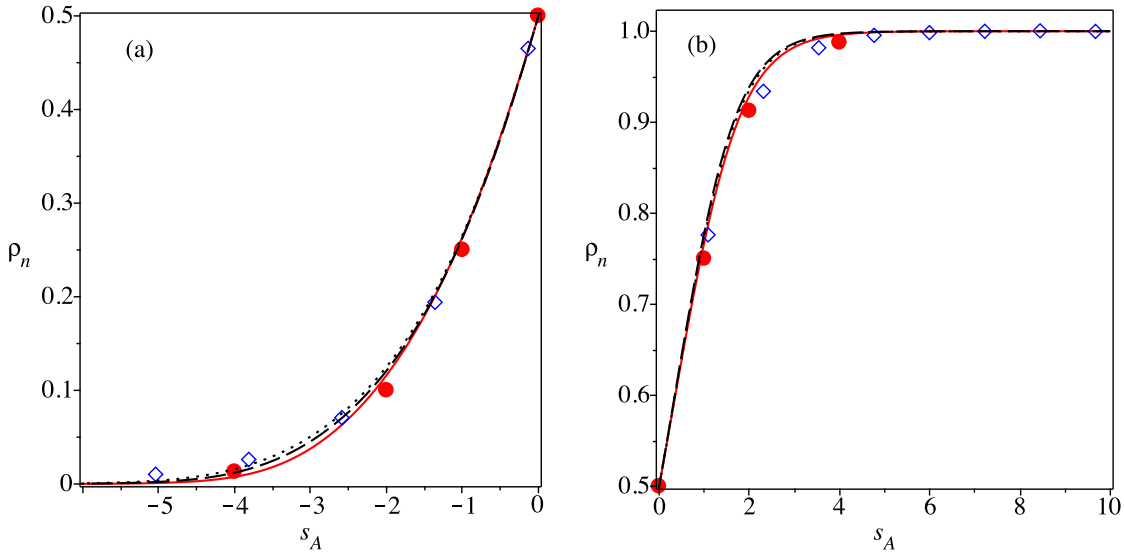

FIG. 5. Normalized density profiles, ρ_n vs s_A, for $M = 3.38$ in two different regions [(a) and (b)]. Solid circles: Experiments [20]; open circles: DSMC for $\sigma = 0.75$ and $\alpha^{-1} = 0.6525$; solid line: NSF; dashed line: LIT2; dotted line: LIT1, where a_2, σ values are given in Table I.

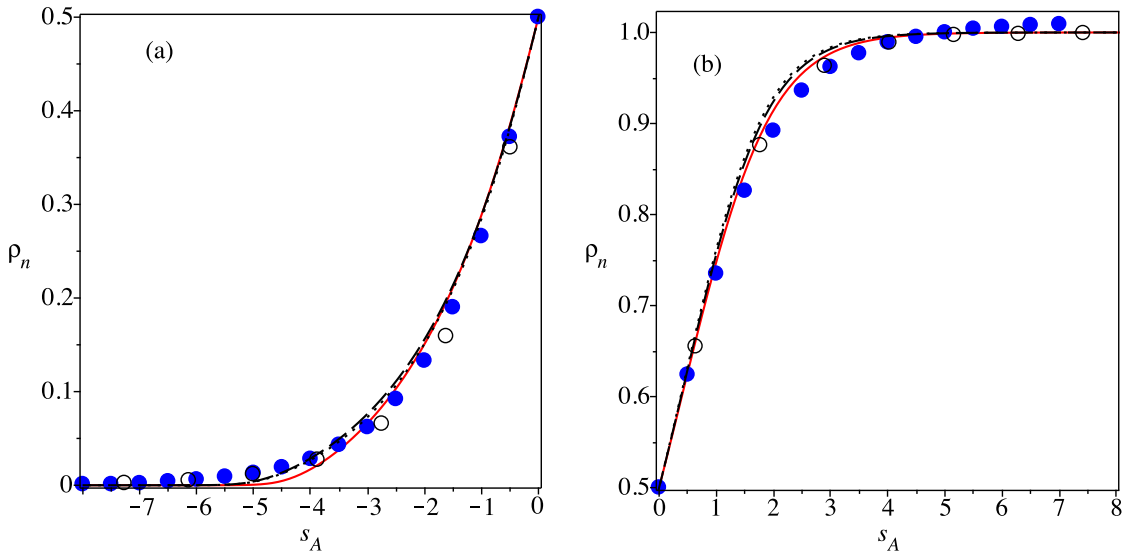

FIG. 6. Normalized density profiles, ρ_n vs s_A, for $M = 8$ in two different regions [(a) and (b)]. Solid circles: Experiments [20]; open circles: DSMC for $\sigma = 0.68$ and $\alpha^{-1} = 0.6015$; solid line: NSF; dashed line: LIT2; dotted line: LIT1, where a_2, σ values are given in Table I.

normalized density profiles for $s_A < 0$, see Figs. 2(d)–2(f). There is an overshoot in the normalized temperature which is shown in Fig. 2(f) and it is apparently model independent since all the different DSMC computations agree with each other in this region; for further discussion on the overshoot see Refs. [51,52].

It is interesting to analyze Bird's DSMC results in the plane v-τ, and they are shown in Fig. 3 for $M = 1.55$ and $M = 9$. The important point to notice is that the DSMC data for different VSS model potentials seem to lie on one line as shown in Figs. 3(a) and 3(b). However, this behavior is only apparent on the large since, as shown in Figs. 3(c) and 3(d), there are deviations from it near down-flow (the hot part of the shock wave), although for $M = 9$ the differences are minor. In addition we have included the result of a hydrodynamic model based on the NSF constitutive equations [1] and the soft-sphere model in which the viscosity is proportional to a power of the temperature; for this case it can be shown that the curve in the v-τ plane is independent of the viscosity-temperature index and in fact independent of the viscosity [1]. We conclude that the curves in the v-τ plane given by the NSF hydrodynamic model are in agreement with those of DSMC for $M = 1.55$ but not for $M = 9$. We will be interested to test the phenomenological model proposed here in this plane. Notice that in Figs. 3(b) and 3(d) the overshoot, mentioned above, is clearly seen.

VII. THE LIT MODEL VS EXPERIMENTAL AND DSMC CALCULATIONS

The experimental data as well as the DSMC calculations allow us to have the criterion to choose the σ viscosity index. This selection has provided a good agreement with the normalizaed density and the NSF model as was shown

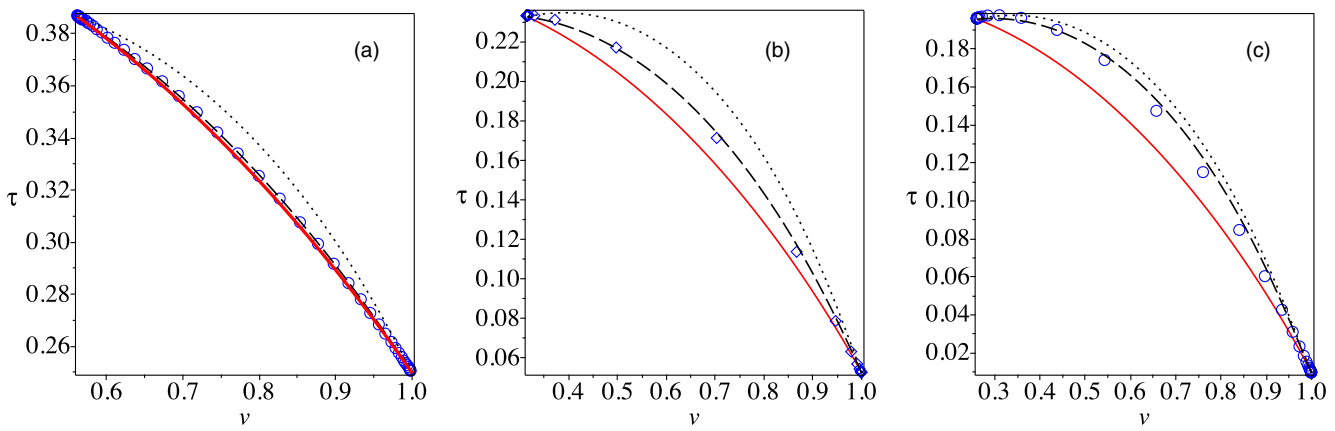

FIG. 7. Orbits, τ vs v, for different Mach numbers. (a) $M = 1.55$. Circles: DSMC for $\sigma = 1.2$ and $\alpha^{-1} = 0.6525$; solid line: NSF; dashed line: LIT2; dotted line: LIT1. (b) $M = 3.38$. Diamonds: DSMC for $\sigma = 0.75$ and $\alpha^{-1} = 0.6525$; solid line: NSF; dashed line: LIT2; dotted line: LIT1. (c) $M = 8$. Circles: DSMC for $\sigma = 0.68$ and $\alpha^{-1} = 0.6015$; solid line: NSF; dashed line: LIT2; dotted line: LIT1, where a_2, σ values are given in Table I.

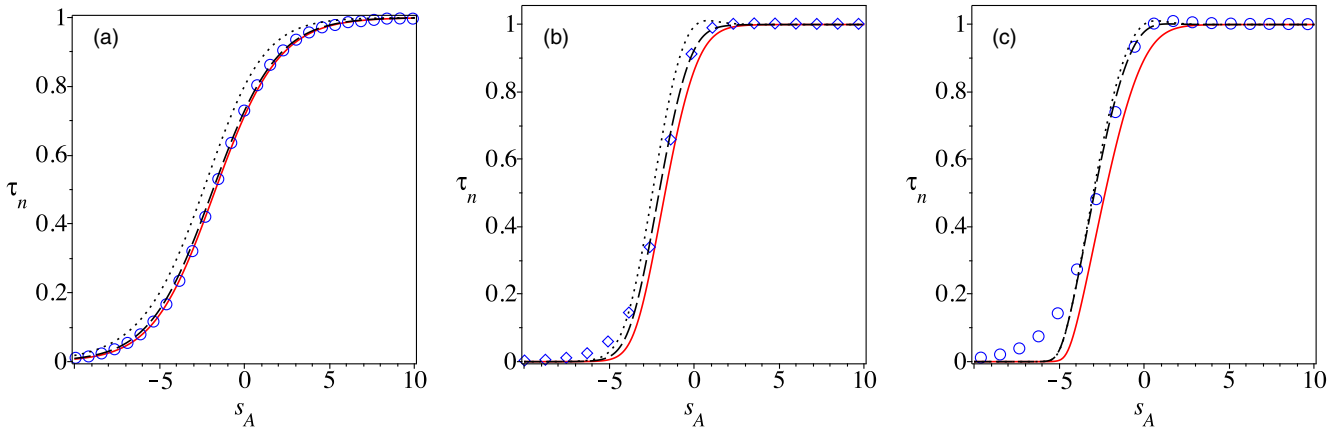

FIG. 8. Normalized temperature profiles, τ_n vs s_A, and different Mach numbers. (a) $M = 1.55$. Circles: DSMC for $\sigma = 1.2$ and $\alpha^{-1} = 0.6525$; solid line: NSF; dashed line: LIT2; dotted line: LIT1. (b) $M = 3.38$. Diamonds: DSMC for $\sigma = 0.75$ and $\alpha^{-1} = 0.6525$; solid line: NSF; dashed line: LIT2; dotted line: LIT1. (c) $M = 8$. Circles: DSMC for $\sigma = 0.68$ and $\alpha^{-1} = 0.6015$; solid line: NSF; dashed line: LIT2; dotted line: LIT1, where a_2, σ values are given in Table I.

recently [1]. However, the orbits were not reproduced completely; moreover, the NSF model is not able to reproduce the qualitative normalized temperature profile. Now we have the LIT model and we need the value for the $a_2(M)$ parameter, which is also obtained by taking into account the DSMC calculations and the experimental data when available (LIT1). The selection of the couple $(\sigma(M),\ a_2(M))$ parameters will drive us to obtain better results than we did with the NSF model (LIT2), a fact that will be shown in the figures below.

First, we consider the normalized density and temperature,

$$\rho_n = \frac{\rho(s) - \rho_0}{\rho_1 - \rho_0}, \quad \tau_n = \frac{\tau(s) - \tau_0}{\tau_1 - \tau_0}, \tag{46}$$

where $\rho(s) = 1/v(s)$. Their calculation will done with the solution of Eqs. (36a) and (36b) with values for $\sigma(M)$ and $a_2(M)$, which will be chosen according to the comparison with DSMC calculations and experimental data when available. Table I gives an example of the set of values we have selected to develop the LIT model. This table presents the values of the parameters needed as well as the calculation of the asymmetry factor and the reciprocal width, properties defined as

$$\overline{Q}_\rho = \frac{\int_{-s}^{0} \rho_n(s')ds'}{\int_0^s [1 - \rho_n(s')]ds'} \quad \text{and} \quad \frac{\lambda_A}{\delta} = \left|\frac{d\rho_n}{ds}\right|_{\max}, \tag{47}$$

which measure different characteristics in the performance of the normalized density profile for the shock wave. In fact, we can say that the reciprocal thickness is local, since it depends on the maximum value for the normalized density derivative, whereas the asymmetry factor is a kind of global measure. In Table I the row called NSF is the best result for the viscosity index to fit the normalized density profile according to the results in Ref. [1]. The DSMC gives the results with Bird's DSMC calculations; the first LIT row (LIT1) for each Mach number gives the best fit of the $a_2(M)$ parameter with the $\sigma(M)$ index fixed with the experimental values for the

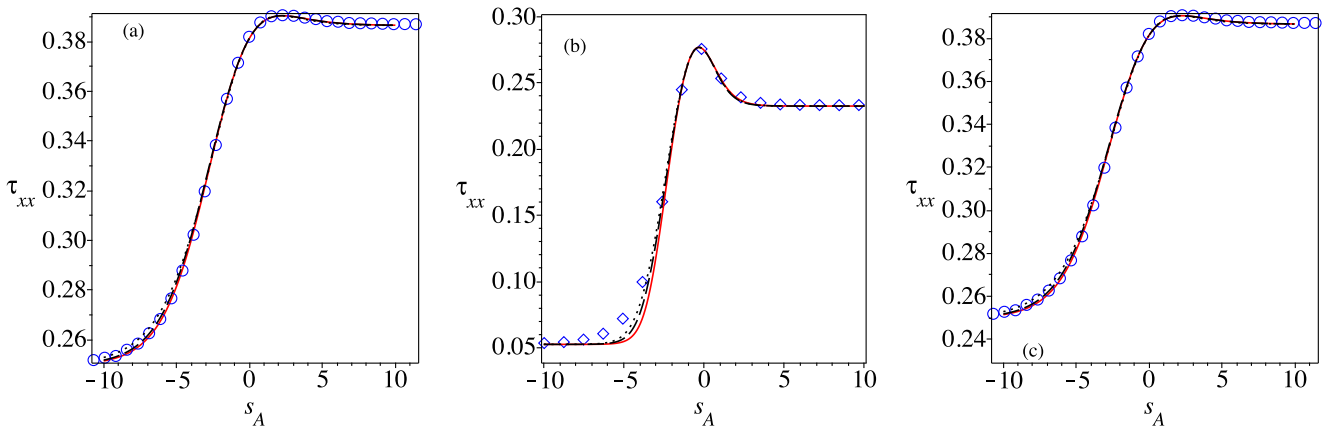

FIG. 9. Reduced longitudinal temperature profiles, τ_{xx} vs s_A, for different Mach numbres. (a) $M = 1.55$. Circles: DSMC for $\sigma = 1.2$ and $\alpha^{-1} = 0.6525$; solid line: NSF; dashed line: LIT2; dotted line: LIT1. (b) $M = 3.38$. Diamonds: DSMC for $\sigma = 0.75$ and $\alpha^{-1} = 0.6525$; solid line: NSF; dashed line: LIT2; dotted line: LIT1. (c) $M = 8$. Circles: DSMC for $\sigma = 0.68$ and $\alpha^{-1} = 0.6015$; solid line: NSF; dashed line: LIT2; dotted line: LIT1, where a_2, σ values are given in Table I.

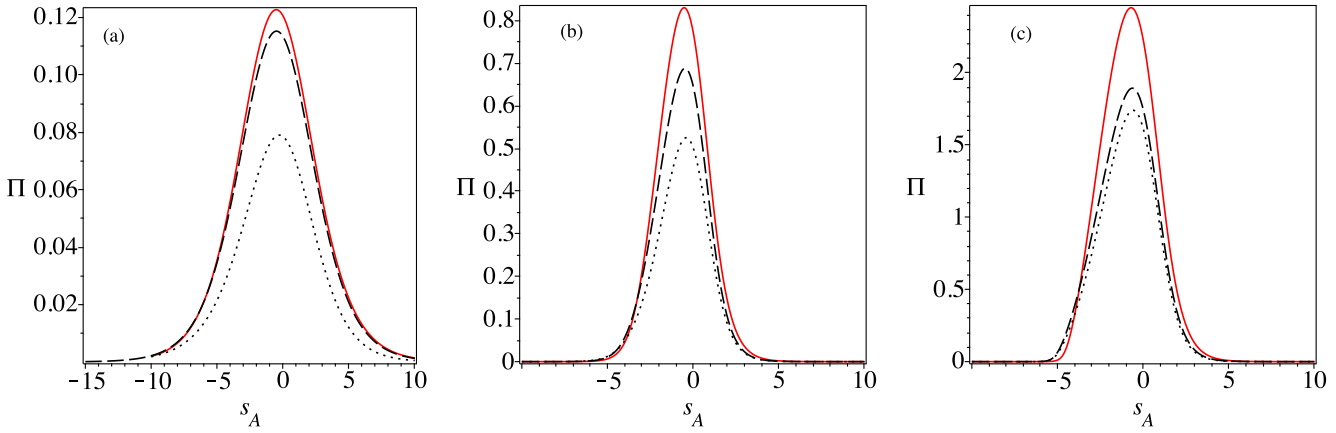

FIG. 10. Reduced viscous pressure tensor profiles, Π vs s_A, for different Mach numbers. (a) $M = 1.55$. Solid line: NSF; dashed line: LIT2; dotted line: LIT1. (b) $M = 3.38$. Solid line: NSF; dashed line: LIT2; dotted line: LIT1. (c) $M = 8$. Solid line: NSF; dashed line: LIT2; dotted line: LIT1, where a_2, σ values are given in Table I.

shear viscosity as measured with other methods independent of shock-wave structure; and, last, the second LIT row (LIT2) reports the best fit for both parameters.

Figures 4–6 show the normalized density profile obtained with the NSF model and two versions of the LIT model for three values of the Mach number. The first version LIT1 takes the viscosity index σ that reproduces the shear viscosity measurements and fits the a_2 parameter to the experimental normalized density profiles, and in the second version LIT2 we fit both the viscosity index σ as well as the a_2 value. Moreover, the results are contrasted with the Alsmeyer experimental data [20] and the DSMC calculations. It should be noted that the first version, LIT1, and the NSF model results are close enough.

The next step in our comparison is done with the orbits in the $v - \tau$ plane, which are obtained by means of solving Eqs. (36). We recall that the orbit does not depend on the viscosity, but it does with the specific values chosen for the $a_2(M)$ parameter, giving a Mach number dependence stronger than in the NSF model. The results are presented in Fig. 7 which deserves several comments to understand completely the meaning of the comparison:

(1) First, we insist on the fact that the orbits equations in both the NSF and LIT models do not depend on the viscosity.

(2) The scale in the vertical axis is different in Figs. 7(a), 7(b), and 7(c) due to the fact that the orbits are calculated between the corresponding equilibrium points and their coordinates are functions of the Mach number.

(3) The NSF model, which only contains the fit in the viscosity index, is good enough only for small Mach numbers.

(4) The LIT model (LIT1) with the experimental value for σ and the fit in the a_2 value (dotted line) is qualitatively better than NSF result.

(5) When the Mach number grows the performance of LIT model with the fit in both parameters (LIT2) is better. The comparison given by the broken line, with the DSMC results represented with the open symbols is the best for all Mach numbers we have tried.

The results for the normalized temperature profile are given in Fig. 8 where the performance of LIT model is qualitatively

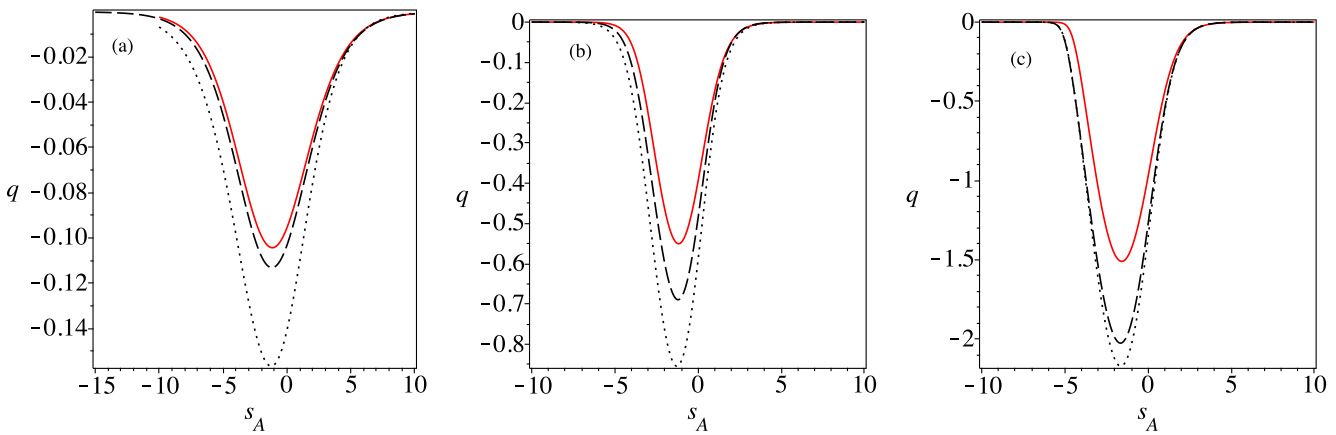

FIG. 11. Reduced heat flux profiles, q vs s_A, for different Mach numbers. (a) $M = 1.55$. Solid line: NSF; dashed line: LIT2; dotted line: LIT1. (b) $M = 3.38$. Solid line: NSF; dashed line: LIT2; dotted line: LIT1. (c) $M = 8$. Solid line: NSF; dashed line: LIT2; dotted line: LIT1, where a_2, σ values are given in Table I.

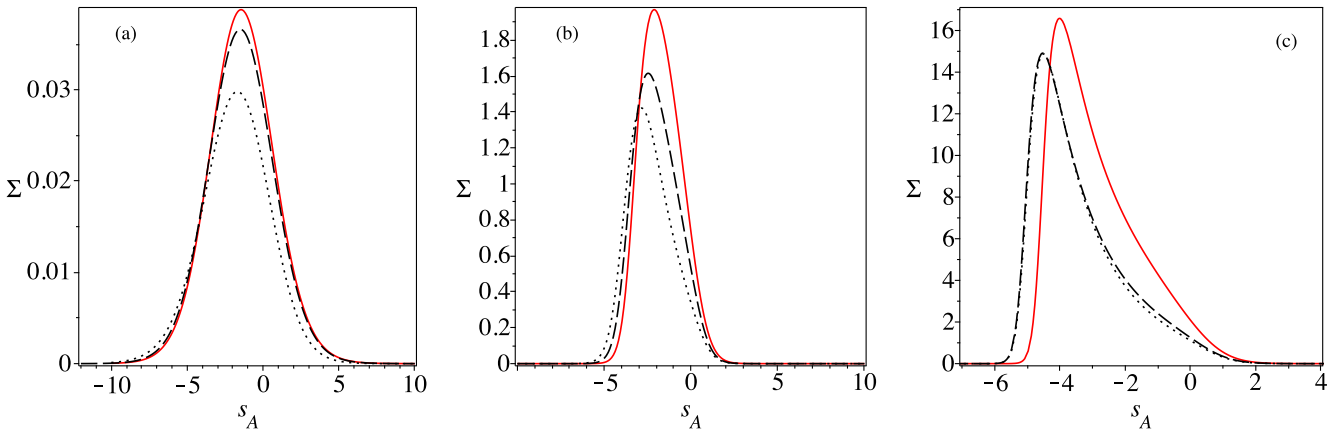

FIG. 12. Reduced entropy production profiles, Σ vs s_A. (a) $M = 1.55$. Solid line: NSF; dashed line: LIT2; dotted line: LIT1. (b) $M = 3.38$. Solid line: NSF; dashed line: LIT2; dotted line: LIT1. (c) $M = 8$. Solid line: NSF; dashed line: LIT2; dotted line: LIT1, where a_2, σ values are given in Table I.

much better than it is for the NSF model. We must recall that there are no experimental results for temperature profiles; the only way to have a criterion comes from the DSMC calculations. Taking this fact into account we see that the overshoot present in DSMC calculations for Mach numbers $M = 3.38,\ 8.0$ is reproduced in the LIT model but it is not with the NSF model.

Some papers in the literature consider the longitudinal temperature as a relevant variable in the studies of shock-wave structure, and we wonder if it plays a role in our treatment [41]. It is defined in terms of the component $P_{xx} = \rho k_B T_{xx}/m$ in the complete pressure tensor, and when it is rewritten in dimensionless variables we obtain

$$\tau_{xx}(s) = v(s)[1 + \tau_0 - v(s)], \tag{48}$$

where we notice that it does not depend explicitly on the transport coefficients; it just depends on the speed. However, a cautionary note must be made, since the speed as a function of s is different for each set of dynamical equations in the model. Figure 9 shows the corresponding calculation for our model compared with the NSF model and DSMC data.

The viscous pressure tensor in LIT model contains the crossed coefficients that we have introduced; then it is interesting to have an insight about their contribution as compared with the NSF calculation. Figure 10 shows the result for three different Mach numbers, where the vertical axis gives the values for the dimensionless viscous component σ_{xx} which is defined as follows:

$$\Pi(s_A) \equiv \frac{\lambda_A \sigma_{xx}}{\eta_0 u_0}. \tag{49}$$

Notice that the vertical scale is different for each Mach number. The maximuum contribution occurs for $s_A \leqslant 0$ and grows with the Mach number.

In a similar way, Fig. 11 represents the heat flux, which also carries the influence of the crossed terms in the LIT model and it is written in the following dimensionless way:

$$q(s_A) = \frac{q_x \lambda_A}{\eta_0 u_0^2}. \tag{50}$$

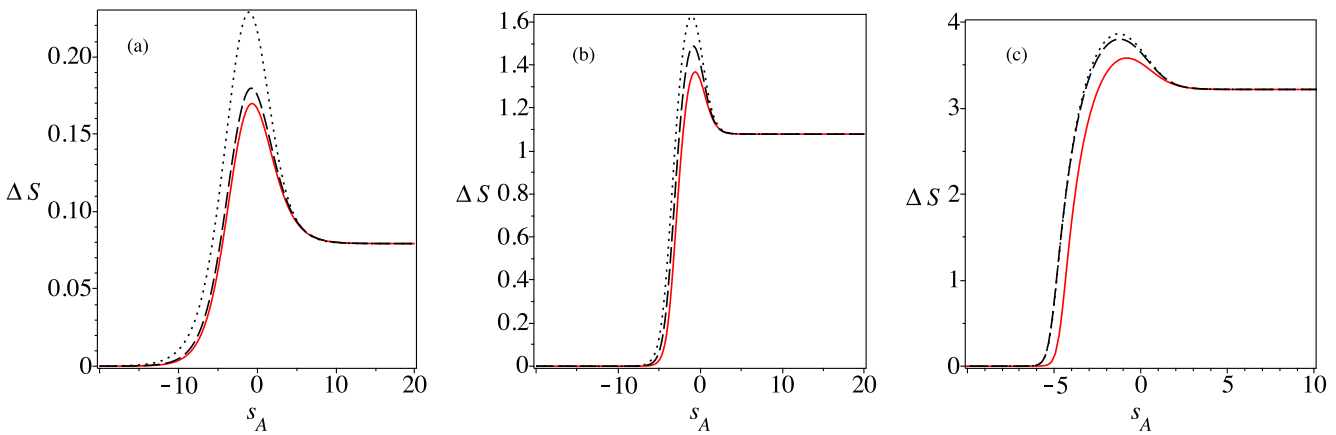

FIG. 13. Reduced entropy change profiles, ΔS vs s_A, for different Mach numbers. (a) $M = 1.55$. Solid line: NSF; dashed line: LIT2; dotted line: LIT1. (b) $M = 3.38$. Solid line: NSF; dashed line: LIT2; dotted line: LIT1. (c) $M = 8$. Solid line: NSF; dashed line: LIT2; dotted line: LIT1, where a_2, σ values are given in Table I.

Now we turn to the entropy production given by Eq. (28), which will written in terms of a dimensionless quantity,

$$\Sigma = \frac{m\lambda_A^2 \Sigma_s}{k_B \eta_0} = \frac{1}{\tau(s_A)}\left[\frac{\tau(s_A)}{\tau_0}\right]^{\sigma} \times \left[-a_1\left(\frac{dv}{ds}\right)^2 - \frac{a_4}{\tau(s_A)}\left(\frac{d\tau}{ds}\right)^2\right]. \quad (51)$$

Figure 12 shows its behavior for three different Mach numbers.

Last, the entropy change as a function of distance, and between the equilibrium points can also be calculated according to the local equilibrium hypothesis. In fact, such a hypothesis has not been altered as a consequence of the change in the constitutive equations; the equation of state and the caloric equation are always valid in this treatment, and then the entropy change taking the up-flow equilibrium point as a reference is calculated in agreement with it and its dimensionless expression is given as

$$\frac{m\,[S(s_A) - S(s_A = 0)]}{k_B} \equiv \Delta S(s_A) = \ln\left\{\left[\frac{\tau(s_A)}{\tau_0}\right]^{3/2} \frac{v(s_A)}{v_0}\right\}, \quad (52)$$

recalling that $v_0 = 1$ at up-flow. Notice that the entropy change between the equilibrium points can be calculated as a function of the Mach number without any reference of the numerical solution obtained with models and it is given as

$$\frac{m\,\Delta S}{k_B} = \ln\left[\left(\frac{\tau_1}{\tau_0}\right)^{3/2}\left(\frac{v_1}{v_0}\right)\right], \quad (53)$$

which must coincide with the difference at the asymptotic values obtained with the numerical solution. Figure 13 shows the behavior of the entropy change for three different Mach numbers.

In Tables II and III we give the results obtained with $M = 3.38$ by means of two independent calculations for all quantities in the figures. Also, in Tables IV and V, the results are given for $M = 8.0$.

TABLE II. Dimensionless variables for $M = 3.38$, LIT2 model with $a_2 = -1.0$, $\sigma = 0.90$.

s_A	ρ_n	τ_n	τ_{xx}	Π	q	Σ	ΔS
−10.0	0.000	0.000	0.053	0.000	0.000	0.000	0.000
−9.0	0.000	0.000	0.053	0.000	0.000	0.000	0.000
−8.0	0.000	0.000	0.053	0.000	0.000	0.000	0.000
−7.0	0.000	0.000	0.053	0.000	0.000	0.000	0.002
−6.0	0.000	0.002	0.053	0.002	−0.003	0.001	0.011
−5.0	0.002	0.015	0.057	0.011	−0.020	0.030	0.068
−4.0	0.012	0.076	0.076	0.056	−0.105	0.462	0.321
−3.0	0.046	0.254	0.130	0.193	−0.333	1.455	0.844
−2.0	0.121	0.519	0.206	0.424	−0.600	1.532	1.301
−1.0	0.263	0.768	0.265	0.646	−0.683	1.072	1.485
0.0	0.500	0.925	0.275	0.647	−0.486	0.530	1.408
1.0	0.778	0.984	0.253	0.352	−0.198	0.119	1.225
2.0	0.939	0.997	0.238	0.104	−0.051	0.010	1.118
3.0	0.987	0.999	0.234	0.023	−0.011	0.001	1.088
4.0	0.997	1.000	0.233	0.005	−0.002	0.000	1.081
5.0	1.000	1.000	0.233	0.001	0.000	0.000	1.079
6.0	1.000	1.000	0.233	0.000	0.000	0.000	1.079
7.0	1.000	1.000	0.233	0.000	0.000	0.000	1.079
8.0	1.000	1.000	0.233	0.000	0.000	0.000	1.079
9.0	1.000	1.000	0.233	0.000	0.000	0.000	1.079
10.0	1.000	1.000	0.233	0.000	0.000	0.000	1.079

TABLE III. Dimensionless variables at $M = 3.38$ with the LIT1 model for $a_2 = -2.5$, $\sigma = 0.72$.

s_A	ρ_n	τ_n	τ_{xx}	Π	q	Σ	ΔS
−10.0	0.000	0.000	0.053	0.000	0.000	0.000	0.000
−9.0	0.000	0.000	0.053	0.000	0.000	0.000	0.000
−8.0	0.000	0.000	0.053	0.000	0.000	0.000	0.001
−7.0	0.000	0.001	0.053	0.001	−0.002	0.000	0.005
−6.0	0.001	0.006	0.054	0.003	−0.008	0.004	0.027
−5.0	0.004	0.029	0.060	0.012	−0.041	0.086	0.134
−4.0	0.016	0.122	0.083	0.049	−0.171	0.711	0.492
−3.0	0.051	0.343	0.137	0.137	−0.460	1.409	1.062
−2.0	0.125	0.636	0.209	0.300	−0.767	1.168	1.495
−1.0	0.266	0.877	0.265	0.481	−0.841	0.701	1.627
0.0	0.500	0.994	0.275	0.502	−0.590	0.339	1.491
1.0	0.774	1.011	0.254	0.284	−0.245	0.086	1.260
2.0	0.935	1.004	0.239	0.088	−0.066	0.008	1.129
3.0	0.985	1.001	0.234	0.020	−0.015	0.000	1.090
4.0	0.997	1.000	0.233	0.004	−0.003	0.000	1.081
5.0	1.000	1.000	0.233	0.001	−0.001	0.000	1.080
6.0	1.000	1.000	0.233	0.000	0.000	0.000	1.079
7.0	1.000	1.000	0.233	0.000	0.000	0.000	1.079
8.0	1.000	1.000	0.233	0.000	0.000	0.000	1.079
9.0	1.000	1.000	0.233	0.000	0.000	0.000	1.079
10.0	1.000	1.000	0.233	0.000	0.000	0.000	1.079

TABLE IV. Dimensionless variables for $M = 8$, LIT2 model with $a_2 = -1.5$, $\sigma = 0.80$.

s_A	ρ_n	τ_n	τ_{xx}	Π	q	Σ	ΔS
−10.0	0.000	0.000	0.009	0.000	0.000	0.000	0.000
−9.0	0.000	0.000	0.009	0.000	0.000	0.000	0.000
−8.0	0.000	0.000	0.009	0.000	0.000	0.000	0.000
−7.0	0.000	0.000	0.009	0.000	0.000	0.000	0.000
−6.0	0.000	0.000	0.010	0.001	−0.002	0.007	0.013
−5.0	0.004	0.033	0.020	0.064	−0.120	9.108	0.750
−4.0	0.029	0.224	0.078	0.387	−0.778	12.388	2.464
−3.0	0.076	0.481	0.154	0.875	−1.543	6.964	0.340
−2.0	0.156	0.718	0.219	1.434	−1.922	4.054	3.724
−1.0	0.289	0.890	0.253	1.850	−1.897	2.415	3.796
0.0	0.500	0.978	0.247	1.749	−1.275	1.248	3.646
1.0	0.757	1.001	0.220	1.008	−0.547	0.348	3.416
2.0	0.924	1.001	0.203	0.335	−0.156	0.037	3.276
3.0	0.982	1.000	0.197	0.082	−0.036	0.002	3.231
4.0	0.996	1.000	0.196	0.018	−0.008	0.000	3.220
5.0	0.999	1.000	0.196	0.004	−0.002	0.000	3.218
6.0	1.000	1.000	0.196	0.001	0.000	0.000	3.217
7.0	1.000	1.000	0.196	0.000	0.000	0.000	3.217
8.0	1.000	1.000	0.196	0.000	0.000	0.000	3.217
9.0	1.000	1.000	0.196	0.000	0.000	0.000	3.217
10.0	1.000	1.000	0.196	0.000	0.000	0.000	3.217

TABLE V. Dimensionless variables for $M = 8$, LIT1 model with $a_2 = -2.0$, $\sigma = 0.76$.

s_A	ρ_n	τ_n	τ_{xx}	Π	q	Σ	ΔS
−10.0	0.000	0.000	0.009	0.000	0.000	0.000	0.000
−9.0	0.000	0.000	0.009	0.000	0.000	0.000	0.000
−8.0	0.000	0.000	0.009	0.000	0.000	0.000	0.000
−7.0	0.000	0.000	0.009	0.000	0.000	0.000	0.000
−6.0	0.000	0.000	0.010	0.001	−0.002	0.006	0.013
−5.0	0.004	0.032	0.195	0.055	−0.116	8.595	0.726
−4.0	0.027	0.226	0.074	0.325	−0.792	12.429	2.483
−3.0	0.073	0.499	0.149	0.747	−1.624	6.748	0.397
−2.0	0.151	0.748	0.216	1.270	−2.130	3.728	3.791
−1.0	0.285	0.922	0.252	1.688	−2.036	2.136	3.853
0.0	0.500	1.001	0.247	1.616	−1.357	1.108	3.679
1.0	0.762	1.010	0.220	0.918	−0.567	0.310	3.425
2.0	0.929	1.004	0.203	0.292	−0.155	0.031	3.276
3.0	0.984	1.001	0.197	0.068	−0.035	0.002	3.230
4.0	0.997	1.000	0.196	0.015	−0.007	0.000	3.220
5.0	0.999	1.000	0.196	0.003	− 0.002	0.000	3.218
6.0	1.000	1.000	0.196	0.001	0.000	0.000	3.217
7.0	1.000	1.000	0.196	0.000	0.000	0.000	3.217
8.0	1.000	1.000	0.196	0.000	0.000	0.000	3.217
9.0	1.001	1.000	0.196	0.000	0.000	0.000	3.217
10.0	1.000	1.000	0.196	0.000	0.000	0.000	3.217

VIII. CONCLUDING REMARKS

The main goal of this paper has been centered in the construction of a model to reproduce the characteristic of the shock-wave structure. Our guide has been the LIT approach, which is a well-known scheme to work with nonequilibrium problems. Recently [1] we have taken the NSF model with a modification which contained an index relating the temperature dependence of the shear viscosity. Such a modification improved in a very good way the performance of the usual Navier-Stokes equations to give an account of some shock-wave properties. In fact, our proposal succeeded in providing good agreement with the experimental normalized density profiles by means of an enhancement of the viscosity. However, we wonder whether it is possible to understand the presence of a viscosity enhancement by means of some other physical mechanism, which can be present in the shock-wave problem due to the anisotrophy in the flow produced by the shock-wave propagation. In order to develop such an idea, this work has taken as a starting point the well-known LIT theory. The new elements in this development include the existence of the crossed terms in the xx component of the viscous tensor and the x component of the heat flux. Moreover, we analyzed the Onsager relations to couple both effects as is usually done in LIT. As a consequence we have obtained that the enhancement we observed in our NSF model can be reproduced by the new model, which is called as LIT1 model, and the perfomance of it is about the same as NSF with regard to the agreement with the normalized density profile. However, we found it necessary to consider a two-parameter model, LIT2, to explain, in addition to the normalized density profiles, the orbit and the qualitative structure of the normalized temperature profile. The detailed comparisons show that the agreement is very good when the fit is done with the viscosity index σ and the crossed coefficient a_2; both are functions of the Mach number. Also, it can be seen that such an agreement is better for Mach numbers near 1, although it is as good for $M = 8$. It is important to emphasize that the LIT2 model is completely phenomenological and its performance agrees in a very good way when compared with experimental and DSMC data, even in a region where we do not expect that a phenomenological model does. Moreover, all other properties such as the viscous tensor and heat flux contributions can be calculated in a straightforward way. The entropy production is non-negative, in agreement with some nonequilibrium versions of the second law of thermodynamics, and shows a maximuum near the center of the profile which can be understood in terms of the maximuun absolute values taken by the fluxes near such a position. Last, the change in the entropy between the equilibrium points also shows a maximum between both steady states, and this point has been discussed recently [57,58].

APPENDIX

Here we provide further details of Bird's implementation of the DSMC method. This method has been developed by G. A. Bird [51,52] and A. L. Garcia [59,60], among many others. It should be pointed out that there are different variants of it and, therefore, it is important to specify the implementation one is using. For a discussion of some variants, see chapter 10 in Ref. [51]. Here we use Bird's 1994 implementation of the shock-wave problem [51]; his DSMC calculations for the shock-wave problem have a long history, see, for example, Ref, [61]. We emphasize that we used his program to generate the DSMC results reported in this work.

As mention by Bird [51,52], the DSMC method can be regarded as a probabilistic physical simulation of flows in

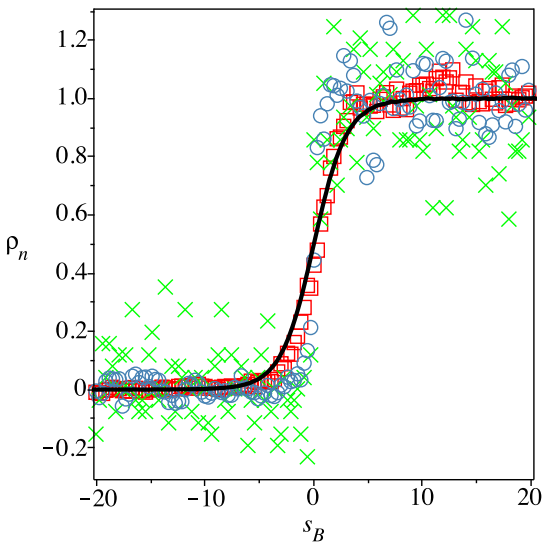

FIG. 14. Normalized density profiles vs Bird's reduced distance, ρ_n vs s_B, for different times. Crosses: DSMC calculation for one time step (whose value is 0.75×10^{-6} s); circles: DSMC calculations for 100 time steps; boxes: DSMC calculations for 1000 time steps; solid line: DSMC calculations for 10 000 time steps.

gases. It considers molecules and their collisions, which are treated in a probabilistic way, to mimic the actual processes that happens in dilute gases and therefore one expects that the results provided by the DSMC method should be related to the Boltzmann equation. That the DSMC method provides a stochastic solution to the Boltzmann equation, for Bird's implementation and under certain conditions, was shown by Wagner in 1992 as mentioned previously [54]. However, as pointed by Bird [52], there are some restrictions that hold for the Boltzmann formulation but are not present in DSMC and it can deal with effects that are beyond the Boltzmann equation. It is not clear, for us, whether this comment refers to monatomic gases in situations where ionization can be neglected or to the phenomenological theory by Larsen-Borhnakke, who included internal degrees of freedom [51]. If they apply to the Boltzmann equation, then one may infer that Bird considers it as an approximation.

To illustrate the convergence properties of DSMC we considered the case of argon using the VHS model ($\alpha = 1$), where its mass is 6.6×10^{-26} kg, its diameter 4.092×10^{-10} m, the temperature of up-flow is taken as 273 K, the number density is 10^{20} atoms/m^3, the viscosity index is equal to $\sigma = 0.81$, and the Mach number is 2. The initial condition for the normalized density profile corresponds to a discontinuous profile at the origin that has the correct Rankine-Hugoniot conditions, and in the case of the normalized density profiles this corresponds to zero for $s_B \equiv x/\lambda_B < 0$, where λ_B is Bird's mean free path given by Eq. (43) and one for $s_B > 0$. In Fig. 14 the behavior of the density profiles calculated by the DSMC method are given for different times. The crosses correspond to the DSMC calculation for one time step, whose value is 0.75×10^{-6} s, the circles for 100 time steps, the boxes correspond to 1000 time steps, and the solid line for 10 000 time steps. In all the DSMC computations we have considered times such that the profiles look smooth and do not change noticeably when the time steps is increased, so that a steady state seems to be reached. For more details on the DSMC method the reader is referred to Refs. [51,52,59,60].

[1] F. J. Uribe and R. M. Velasco, Phys. Rev. E **97**, 043117 (2018).
[2] S. Chapman and T. G. Cowling, *The Mathematical Theory of Non-Uniform Gases* (Cambridge University Press, Cambridge, 1970).
[3] A. V. Bobylev, M. Bisi, M. P. Cassinari, and G. Spiga, Phys. Fluids **23**, 030607 (2011).
[4] L. S. García-Colín, R. M. Velasco, and F. J. Uribe, Phys. Rep. **465**, 149 (2008).
[5] M. S. Shavaliyev, J. Appl. Maths Mech. **57**, 573 (1993).
[6] J. M. Reese, L. C. Woods, F. J. P. Thivet, and S. M. Candel, J. Comput. Phys. **117**, 240 (1995).
[7] H. Grad, Commun. Pure Appl. Math. **5**, 257 (1952).
[8] M. Torrilhon, Annu. Rev. Fluid Mech. **48**, 429 (2016).
[9] T. Ruggeri, Phys. Rev. E **47**, 4135 (1993).
[10] M. Y. Timokhin, Y. A. Bondar, A. A. Kokhanchik, M. S. Ivanov, I. E. Ivanov, and I. A. Kryukov, Phys. Fluids **27**, 037101 (2015).
[11] R. K. Agarwal, K. Y. Yun, and R. Balakrishnan, Phys. Fluids **13**, 3061 (2001).
[12] M. Y. Timokhin, H. Struchtrup, A. A. Kokhanchik, and Y. A. Bondar, Phys. Fluids **29**, 037105 (2017).
[13] W. Gustafson, Phys. Fluids **3**, 732 (1960).
[14] H. M. Mott-Smith, Phys. Rev. **82**, 885 (1951).
[15] M. A. Solovchuk and T. W. H. Sheu, Phys. Rev. E **81**, 056314 (2010).
[16] E. P. Muntz and N. L. Harnett, Phys. Fluids **12**, 2027 (1969).
[17] F. J. Uribe, W. G. Hoover, and C. G. Hoover, Comput. Methods Sci. Technol. **19**, 5 (2013).
[18] F. J. Uribe, R. M. Velasco, and L. S. García-Colín, Phys. Rev. E **58**, 3209 (1998).
[19] K. Xu and Z. Guo, J. Comput. Math. **29**, 639 (2011).
[20] H. Alsmeyer, J. Fluid Mech. **74**, 497 (1976).
[21] D. Gilbarg, Am. J. Math. **73**, 256 (1951).
[22] B. S. Schmidt, J. Fluid Mech. **39**, 361 (1969).
[23] D. Gilbarg and D. Paolucci, J. Ration. Mech. Anal. **2**, 617 (1953).
[24] K. Xu and E. Josyula, Commun. Comput. Phys. **1**, 425 (2006).
[25] B. L. Holian, M. Mareschal, and R. Ravelo, Phys. Rev. E **83**, 026703 (2011).
[26] B. L. Holian, M. Mareschal, and R. Ravelo, in *Shock Compression of Condensed Matter–2011*, Parts 1 and 2, edited by M. L. Elert and W. T. Buttler and J. P. Borg and J. L. Jordan and T. J. Vogler, AIP Conf. Proc. No. 1426 (American Physical Society, New York, 2012), pp. 1215–1218.
[27] F. J. Uribe, Phys. Rev. E **93**, 033110 (2016).
[28] K. A. Fiscko and R. D. Chapman, in *Rarefied Gas Dynamics*, edited by E. P. Muntz, D. P. Weaver, and D. H. Campbell (AIAA, Washington, 1989), 374–395.
[29] W. Zhao and W. Chen, Int. J. Nonlin. Sci. Numer. Simul. **14**, 493 (2013).
[30] H. Brenner, Physica A **349**, 60 (2005).
[31] H. Brenner, Physica A **388**, 3391 (2009).
[32] C. J. Greenshields and J. M. Reese, J. Fluid Mech. **580**, 407 (2007).
[33] F. J. Uribe, in *Coping with Complexity: Model Reduction and Data Analysis*, edited by A. N. Gorban and D. Roose (Springer–Verlag, Berlin, 2011), 207–229.
[34] D. Jou, J. Casas-Vázquez, and G. Lebon, Rep. Prog. Phys. **62**, 1035 (1999).
[35] D. Jou and D. Pavón, Phys. Rev. A **44**, 6496 (1991).
[36] D. Jou, J. Casas-Vázquez, and G. Lebon, *Extended Irreversible Thermodynamics* (Springer–Verlag, Berlin, 1993).
[37] M. AlGhoul and B. C. Eu, Phys. Rev. E **56**, 2981 (1997).
[38] B. Eu, *Nonequilibrium Statistical Mechanics* (Kluwer, Dordrecht, 1998).
[39] R. S. Myong, J. Comput. Phys. **168**, 47 (2001).
[40] B. L. Holian, Phys. Rev. A **37**, 2562 (1988).
[41] B. L. Holian, C. W. Patterson, M. Mareschal, and E. Salomons, Phys. Rev. E **47**, R24(R) (1993).
[42] B. L. Holian and M. Mareschal, Phys. Rev. E **82**, 026707 (2010).
[43] Y.-G. He, X.-Z. Tang, and Y.-K. Pu, Phys. Rev. E **78**, 017301 (2008).
[44] S. R. de Groot and P. Mazur, *Nonequilibrium Thermodynamics* (North Holland, Amsterdam, 1962).

[45] Y. B. Zel'dovich, and Y. P. Raizer, *Physics of Shock Waves and High-Temperature Hydrodynamic Phenomena* (Dover, New York, 2002).
[46] G. I. Barenblatt, *Scaling, Self–Similarity, and Intermediate Asymptotics* (Cambridge, New York, 2009).
[47] J. Keizer, *Statistical Thermodynamics of Nonequilibrium Processes* (Springer–Verlag, New York, 1987).
[48] W. G. Hoover, Phys. Rev. Lett. **42**, 1531 (1979).
[49] E. Salomons and M. Mareschal, Phys. Rev. Lett. **69**, 269 (1992).
[50] B. D. Coleman and M. E. Gurtin, J. Chem. Phys. **47**, 597 (1967).
[51] G. A. Bird, *Molecular Gas Dynamics and the Direct Simulation of Gas Flows* (Oxford-Clarendon, New York, 1994).
[52] G. A. Bird, *The DSMC Method (Ver. 1.2)* (CreateSpace Independent Publishing Platform, Lexington, KY, USA, 2013).
[53] N. Metropolis, A. W. Rosenbluth, M. N. Rosenbluth, A. H. Teller, and E. Teller, J. Chem. Phys. **21**, 1087 (1953).
[54] W. Wagner, J. Stat. Phys. **66**, 1011 (1992).
[55] F. Sharipov and C. Dias, Comput. Fluids **150**, 115 (2017).
[56] F. Sharipov and J. L. Strapasson, Phys. Fluids **24**, 011703 (2012).
[57] L. G. Margolin, Entropy **19**, 368 (2017).
[58] L. G. Margolin, J. M. Reisner, and P. M. Jordan, Int. J. Non-Linear Mech. **95**, 333 (2017).
[59] A. L. Garcia, *Numerical Methods for Physics*, 2nd ed. (Prentice Hall, Upper Saddle River, NJ, 2000).
[60] A. L. Garcia, *Numerical Methods for Physics (Python)* (CreateSpace Independent Publishing Platform, San Bernardino, CA, USA, 2017).
[61] G. A. Bird, Phys. Fluids **13**, 1172 (1970).